



การวิเคราะห์หาความสูงของฐานเมฆโดยใช้แบบจำลองทางอุตุนิยมวิทยา:
กรณีศึกษาจังหวัดเชียงใหม่

CLOUD BASE HEIGHT DETERMINATION BY METEOROLOGICAL MODEL
SIMULATION: THE CASE STUDY OF CHIANG MAI

PIYAON SAPPHAPHAB

GRADUATE SCHOOL Srinakharinwirot University

2018

การวิเคราะห์หาความสูงของฐานเมฆโดยใช้แบบจำลองทางอุตุนิยมวิทยา:
กรณีศึกษาจังหวัดเชียงใหม่



ปริญญานิพนธ์นี้เป็นส่วนหนึ่งของการศึกษาตามหลักสูตร
การศึกษามหาบัณฑิต สาขาวิชาฟิสิกส์
คณะวิทยาศาสตร์ มหาวิทยาลัยศรีนครินทรวิโรฒ
ปีการศึกษา 2561
ลิขสิทธิ์ของมหาวิทยาลัยศรีนครินทรวิโรฒ

CLOUD BASE HEIGHT DETERMINATION BY METEOROLOGICAL MODEL
SIMULATION: THE CASE STUDY OF CHIANG MAI



A Thesis Submitted in partial Fulfillment of Requirements
for MASTER OF EDUCATION (Physics)
Faculty of Science Srinakharinwirot University

2018

Copyright of Srinakharinwirot University

THE THESIS TITLED
CLOUD BASE HEIGHT DETERMINATION BY METEOROLOGICAL MODEL
SIMULATION: THE CASE STUDY OF CHIANG MAI

BY
PIYAON SAPPHAPHAB

HAS BEEN APPROVED BY THE GRADUATE SCHOOL IN PARTIAL FULFILLMENT OF
THE REQUIREMENTS FOR THE MASTER OF EDUCATION IN PHYSICS
AT SRINAKHARINWIROT UNIVERSITY

..... Dean of Graduate School
(Assoc. Prof. Dr. Chatchai Ekpanyaskul, MD.)
.....

ORAL DEFENSE COMMITTEE

..... Major-advisor Chair
(Asst. Prof. Dr.SIRILUK RUANGRUNGROTE) (Prof. Dr.Pichet Limsuwan)

..... Committee
(Assoc. Prof. Dr.Pongkaew
Udomsamuthirun)

| | |
|----------------|--|
| Title | CLOUD BASE HEIGHT DETERMINATION BY METEOROLOGICAL MODEL SIMULATION: THE CASE STUDY OF CHIANG MAI |
| Author | PIYAON SAPPHAPHAB |
| Degree | MASTER OF EDUCATION |
| Academic Year | 2018 |
| Thesis Advisor | Assistant Professor Dr. SIRILUK RUANGRUNGROTE |

This thesis investigated CBH over Omkoi, Chiang Mai in the north of Thailand from three different methods; ground-based instrument, meteorological model simulation, and satellite-based observation including a ceilometer, a SkewT/LogP diagram and the MODIS satellite, respectively. A ceilometer can measure up to four adjacent CBH layers and provided CVS over this site. It showed that the largest number of detected layers accounted for single-layered clouds, and the CBH distributions were dominated by low and middle clouds. In addition, CBH in the rainy season was the most complicated, in comparison with other seasons. Also, the CBH derived from ceilometer and SkewT/LogP diagram were compared to validating and evaluating the performance of each approach. The CBH at CCL was more reliable than the one received from LCL at $MBD = 7.906$ and $R^2 = 0.281$. Moreover, the CBH was compared to and derived from ceilometers and the MODIS satellite. Although we cannot directly obtain CBH from MODIS, there was an available algorithm instead. It was remarked that the algorithm was valid for low- and mid-level clouds. Thus the comparison of the CBH at that level (approximately under three kilometers) with those obtained by the other two instruments, and results showed the best fit with MBD was equal to 19.194 and $R^2 = 0.700$.

Keyword : cloud base height, cloud vertical structure, ceilometer, SkewT/LogP diagram, MODIS

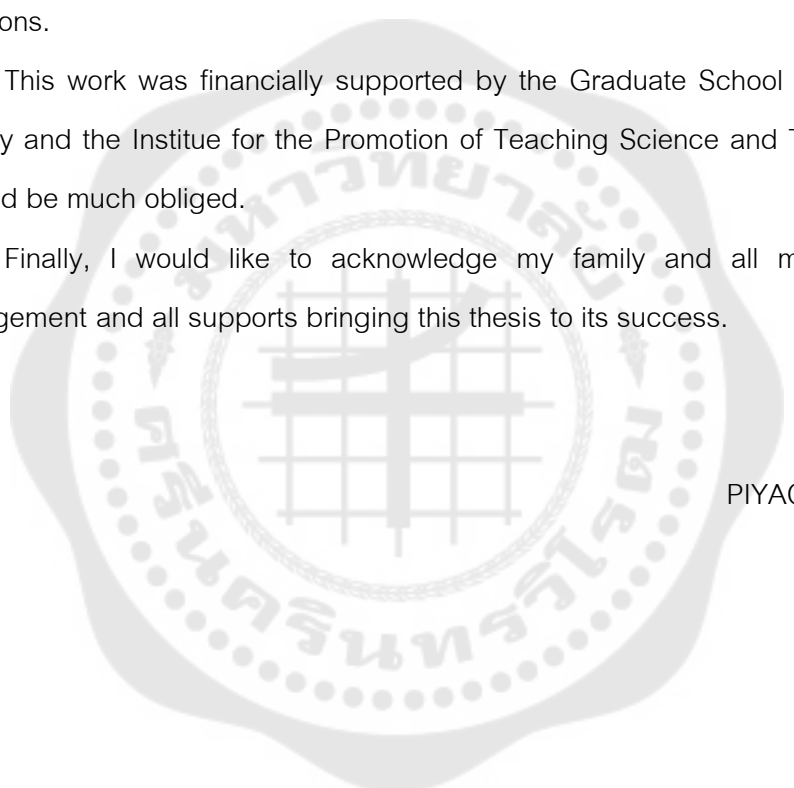
ACKNOWLEDGEMENTS

Firstly, I would like to appreciate Asst. Prof. Dr. Siriluk Ruangrungle, my adviser, for meaningful guidance, comments, and devoted time to carry on this research.

I am exceedingly grateful to the Solar Energy Research Laboratory (SERL), Department of Physics, Faculty of Science, Silpakorn University and the Royal Rainmaking and Agricultural Aviation Department for providing the really useful database and helpful suggestions.

This work was financially supported by the Graduate School of Srinakharinwirot University and the Institute for the Promotion of Teaching Science and Technology (IPST), so I would be much obliged.

Finally, I would like to acknowledge my family and all my friends for the encouragement and all supports bringing this thesis to its success.



PIYAON SAPPHAPHAB

TABLE OF CONTENTS

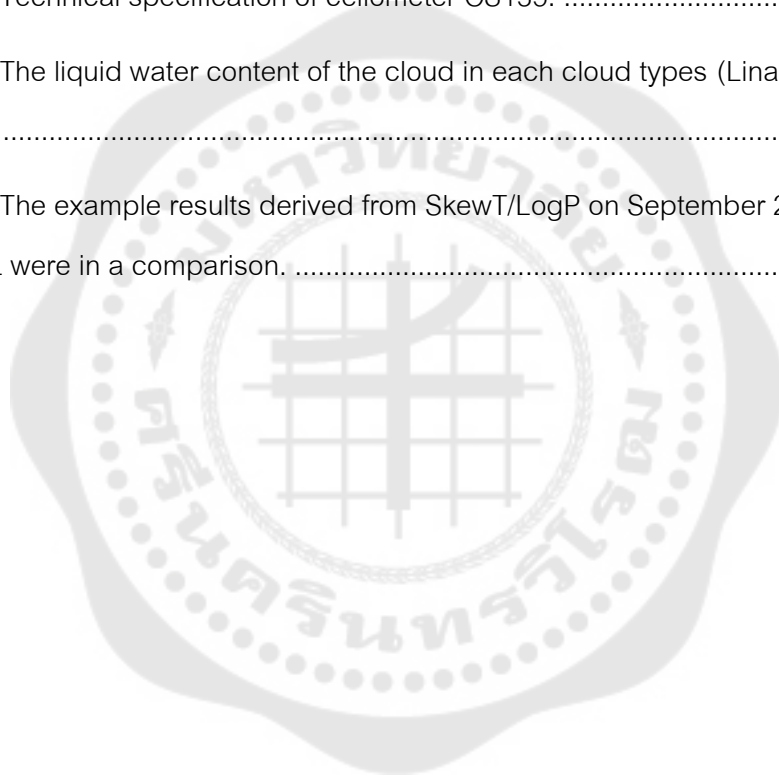
| | Page |
|---|------|
| ABSTRACT | D |
| ACKNOWLEDGEMENTS..... | E |
| TABLE OF CONTENTS..... | F |
| LIST OF TABLES..... | I |
| LIST OF FIGURES | J |
| CHAPTER 1 Introduction..... | 1 |
| Background..... | 1 |
| Objectives of the research..... | 4 |
| Significance of the research | 4 |
| Scope of this work..... | 4 |
| Research Hypotheses..... | 4 |
| List of abbreviations | 5 |
| CHAPTER 2 Literatures review and theoretical background | 6 |
| 1. Earth's atmosphere | 6 |
| 1.1 Troposphere | 6 |
| 1.2 Stratosphere | 6 |
| 1.3 Mesosphere..... | 7 |
| 1.4 Thermosphere | 7 |
| 2. Clouds | 8 |
| 2.1 Stable and unstable air | 8 |
| 2.2 Cloud formation | 9 |

| | |
|--|----|
| 2.3 Lifting processes that form clouds (Ackerman & Knox, 2007; Met office, 2018) | 10 |
| 2.4 Cloud Composition (Ackerman & Knox, 2007; Bureau of meteorology, 2018) | 16 |
| 2.5 Types of cloud (Funk, n.d.; Julian Mayers & Hughes, 2004) | 18 |
| 2.6 Atmospheric scattering (Nave, n.d.) | 30 |
| 3. Cloud observations | 31 |
| 3.1 Cloud amount observation | 31 |
| 3.2 CBH observation | 32 |
| 3.3 CBH observation methods | 33 |
| 4. Relevant research | 42 |
| CHAPTER 3 Research methodology | 44 |
| 1. Framework | 44 |
| 2. Research methods | 45 |
| 2.1 Ceilometer | 45 |
| 2.2 SkewT/LogP diagram | 46 |
| 2.3 MODIS Satellite | 47 |
| 3. Research Site and Data collection | 49 |
| 3.1 Research Site | 49 |
| 3.2 Data collection | 50 |
| 4. Data analysis | 50 |
| 4.1 Cloud vertical structure (CVS) | 51 |
| 4.2 The CBH distributions | 51 |
| 4.3 The distance between adjacent CBH | 51 |

| | |
|---|----|
| 4.4 Comparison of CBH obtained from ceilometer and SkewT/LogP diagram | 51 |
| 4.5 Comparison of CBH obtained from ceilometer and MODIS | 51 |
| 5. Statistic validation | 52 |
| 5.1 Comparison of CBH obtained from ceilometer and SkewT/LogP diagram..... | 52 |
| 5.2 Comparison of CBH obtained from ceilometer and MODIS..... | 53 |
| CHAPTER 4 Results and discussions | 55 |
| 4.1 Cloud vertical structure (CVS) | 55 |
| 4.2 The CBH distributions | 56 |
| 4.3 The distance between adjacent CBH..... | 67 |
| 4.4 Comparison of CBH obtained from ceilometer and SkewT/LogP diagram | 68 |
| 4.5 Comparison of CBH obtained from ceilometer and MODIS | 70 |
| CHAPTER 5 Conclusion remarks | 76 |
| 5.1 Conclusion remarks | 76 |
| 5.2 Future works..... | 79 |
| REFERENCES..... | 80 |
| VITA | 85 |

LIST OF TABLES

| | Page |
|--|------|
| Table 1. The effect of stable and unstable air on cloud form | 9 |
| Table 2. The composition of each cloud type..... | 17 |
| Table 3. The estimation of cloud amounts | 32 |
| Table 4. Technical specification of ceilometer CS135. | 45 |
| Table 5. The liquid water content of the cloud in each cloud types (Linacre & Geerts, n.d.)..... | 48 |
| Table 6. The example results derived from SkewT/LogP on September 2016 when LCL and CCL were in a comparison. | 70 |



LIST OF FIGURES

| | Page |
|---|------|
| Figure 1. Structure of atmosphere (Russell, 2018) | 8 |
| Figure 2. Four lifting processes that develop cloud (a) Convection, (b) Orographic lifting, (c) Frontal lifting, and (d) Convergence (Newman, 2006) | 11 |
| Figure 3. Weather front symbols (a) warm front, (b) cold front, (c) occluded front, and (d) stationary front | 13 |
| Figure 4. A cross section through cold front (Ackerman & Knox, 2007) | 13 |
| Figure 5. Vertical slice through warm front (Ackerman & Knox, 2007) | 14 |
| Figure 6. Occluded front (a) Cold-type occluded front, (b) Warm-type occluded front (Ackerman & Knox, 2007) | 15 |
| Figure 7. Type of clouds (Ackerman & Knox, 2007) | 18 |
| Figure 8. Cirrus cloud (Schumacher, 2007) | 19 |
| Figure 9. Cirrostratus clouds (Mecelis, 2015) | 20 |
| Figure 10. Cirrocumulus clouds (Everson, 2017) | 21 |
| Figure 11. Altostratus clouds (Gudd, 2016) | 22 |
| Figure 12. Altocumulus clouds (Omdal, 2016) | 22 |
| Figure 13. Stratus clouds (Knapp, 2014) | 23 |
| Figure 14. Stratocumulus clouds (Bruhn, 2006) | 24 |
| Figure 15. Nimbostratus clouds (Sugi, 2013) | 24 |
| Figure 16. Cumulus clouds (Linehan, 2010) | 25 |
| Figure 17. Cumulonimbus clouds (Favre, 2016) | 25 |
| Figure 18. Wall cloud (Penry, 2013) | 26 |

| | |
|---|----|
| Figure 19. Shelf cloud (Thompson et al., 2013)..... | 27 |
| Figure 20. Fractus (Bruhn, 2010) | 27 |
| Figure 21. Mammatus (Dorr, 2018) | 28 |
| Figure 22. Contrail (Theberge, 2018)..... | 28 |
| Figure 23. Fog (Schwemmer, 2013)..... | 29 |
| Figure 24. The difference of Rayleigh scattering and Mie scattering (Nave, n.d.) | 30 |
| Figure 25. Isobars on SkewT/LogP diagram..... | 34 |
| Figure 26. Isotherms on SkewT/LogP diagram..... | 35 |
| Figure 27. Dry adiabats on SkewT/LogP diagram | 36 |
| Figure 28. Saturation mixing ratio on SkewT/LogP diagram..... | 37 |
| Figure 29. CCL and LCL on SkewT/LogP diagram (Ceilometers Net, 2015)..... | 38 |
| Figure 30. Ceilometer single lens overlap geometry modified from (Ceilometers Net, 2015)..... | 40 |
| Figure 31. Terra spacecraft (NASA, 2017) | 41 |
| Figure 32. Aqua spacecraft (NASA, 2018) | 41 |
| Figure 33. Research framework | 44 |
| Figure 34. Display of Viewpoint software | 46 |
| Figure 35. Campbell Scientific ceilometer CS135 (Campbell scientific, 2018) | 46 |
| Figure 36. Display of SkewT/LogP diagram from Department of Royal Rainmaking and Agricultural Aviation website | 47 |
| Figure 37. The location of Chiang Mai province, Northern of Thailand modified from | 50 |
| Figure 38. The frequency (%) of CBH aggregated layers, four-layered (red), three-layered (yellow), two-layered (grey), and single-layered (blue)..... | 55 |

| | |
|--|----|
| Figure 39. The frequency (%) of CBH aggregated layers, four layers (red), three-layered (yellow), two-layered (grey), and single-layered (blue) in different seasons | 56 |
| Figure 40. The CBH distribution frequency in September 2016 to December 2017 for all layers system..... | 57 |
| Figure 41. The CBH distribution frequency in September 2016 to December 2017 for multi-layered systems (three layers system)..... | 58 |
| Figure 42. The CBH distribution frequency in September 2016 to December 2017 for multi-layered system (two layers system) | 59 |
| Figure 43. The CBH distribution frequency in September 2016 to December 2017 for the only first layers system | 60 |
| Figure 44. The CBH distributions in different seasons | 61 |
| Figure 45. The single day variation of CBH in winter on November 25, 2017 | 63 |
| Figure 46. The single day variation of CBH in summer on April 23, 2017 | 64 |
| Figure 47. The single day variation of CBH in rainy on September 15, 2016 | 65 |
| Figure 48. The variation of CBH characteristics during morning (06:30-07:30 LCT)..... | 66 |
| Figure 49. The frequency of distance between adjacent CBH for multilayers system | 67 |
| Figure 50. The linear correlation between CBH retrieved from ceilometer vs. cloud simulation at LCL 50 mb..... | 69 |
| Figure 51. The linear correlation between CBH retrieved from ceilometer vs. cloud simulation at CCL 50 mb | 69 |
| Figure 52. The received example result, cloud effective radius, by a) Terra and b) Aqua on December 30, 2017 at different time | 71 |
| Figure 53. The linear correlation between CBH retrieved from ceilometer vs. MODIS.... | 72 |
| Figure 54. The linear correlation between CBH retrieved from ceilometer vs. MODIS when we considered CBH at low level | 73 |

Figure 55. The comparison of CBH distribution collected by ceilometer and MODIS on September 3, 2016..... 74

Figure 56. The comparison of CBH distribution collected by ceilometer and MODIS on September 22, 2016..... 75



CHAPTER 1

Introduction

Background

Clouds are an aggregation of tiny water droplets or frozen crystals of water floating in the sky. Clouds are important material of the Earth's atmospheric system. Clouds can affect the Earth's radiation budget and present complicated interactions with the other atmospheric components (Tzoumanikas et al., 2016). Moreover, characteristics and compositions of cloud indicate the condition of atmospheric motion, and monitoring these parameters has an essential implications for weather forecast, climate modeling, and aeronautics (Wang et al., 2018). To understand their full impact and receiving accurate information, it is crucial to consider cloud properties such as cloud base height (CBH), cloud vertical structure (CVS), and vertical frequency of cloud occurrence (CVF) (Lee et al., 2018).

Historically, these cloud properties have been recorded by human observers for over 100 years. With the progress of the automated meteorological measurement technology, many instruments i.e. the ceilometer have been developed and improved to obtain these cloud properties. (Liu et al., 2015)

However, there is a further need for development of automatic cloud observation and continuous cloud description for climatological issues. Also, more information about cloud characteristics, behaviors, and the phenomenons in which clouds take part, are needed. (Costa-Surós et al., 2013). Guichard and Couvreux realize the limitation of cloud observations, only limited insight can be gained from analytical approaches because of the very nature of the processes. This may not enough to provide exact answers to the numerous questions (Guichard & Couvreux, 2017).

Several methods are employed for detecting and determining cloud characteristics, these approaches may be classified into three types; ground-based measurement, meteorological model simulation, and satellite-based observation (Forsythe et al., 2000).

For ground-based measurement, ceilometer is the most common instrument mainly chosen to determine the CBH. Ceilometer is a single-wavelength backscatter LIDAR which emit wavelength in the near infrared between 900 and 1100 nm to avoid strong Rayleigh scattering. Its pulse repetition rate is on the order of a few kHz, and the pulse energy of the laser is sufficiently low to allow eye-safe operation. Ceilometer provides a continuous record of CBH with high temporal and spatial resolutions (Wiegner et al., 2014).

Next, meteorological model simulation, cloud simulation became more popular for explaining character of clouds. In recent studies found that modeling virtual clouds is a difficult task to do. Generally, cloud formation relies on the laws of fluid mechanics and thermodynamics or on procedural techniques which is a chaotic process depending strongly on initial conditions. Most physically-based methods involve solving partial differential equation (PDEs), in particular, the Navier-Stokes equations, which cost in computational terms (Duarte & Gomes, 2017; Wither et al., 2008).

The Skew-T, Log-P diagram, a kind of cloud simulation, is the standard method using in meteorology in worldwide, including Thailand. This diagram is a sketch of meteorological parameter obtained from an upper air sounding (vertical measurement), radiosonde, in a manner such that the basic atmospheric energy transformations are visually depicted. According to this diagram, the real time meteorological parameters received from an upper air sounding are plotted. The Skew-T, Log-P diagram presents a vertical picture of the atmospheric conditions at the time of observation and allows for computations of various parameters required by user, especially for meteorologists. The Skew-T, Log-P diagram is preferable because (a) The important isopleths are straight rather than curved which makes it easier to estimate, (b) The angle between the adiabats and isotherms is large enough to facilitate estimates of the stability, (c) The ratio of area on the chart to thermodynamic energy is the same value the whole diagram, (d) an entire sounding to levels in the stratosphere can be plotted on one chart, and (e) the vertical coordinate of the diagram estimates the vertical in the atmosphere (i.e. the isobars are plotted to a logarithmic scale and pressure in the atmosphere decreases

nearly logarithmically with height) (AIR WEATHER SERVICE SCOTT AFB IL., 1990; Mcmurdie, 2007).

Costa-Surós recommended that ceilometer measurement and radiosonde estimation methods should be compared for better describing Earth's atmosphere (Costa-Surós et al., 2013).

As satellite-based instrumentation, the instruments onboard satellites such as Cloud-Aerosol Lidar and Infrared Pathfinder Satellite Observation (CALIPSO), or CloudSat, provide the cloud structure information. The horizontal extent of the upper layer or single layer of clouds is well observed by satellite. On the other hand, ground-based observations cannot provide any information on cloud top height (CTH), optical thickness or their horizontal boundary. However, satellite-based measurements are widely used to detect several cloud properties. Sharma reveals the algorithms for deriving CBH which is received physical parameters from MODIS (Moderate Resolution Imaging Spectroradiometer) satellite. MODIS provides measurements of large-scale global dynamics, including cloud cover, radiation budget, and the processes occurring in the lower atmosphere at 5 kilometers spatial resolution. (Forsythe et al., 2000; L'Ecuyer & Jiang, 2010; Sharma et al., 2016).

Due to their limitation of satellite-based and ground-based observation, Stefan and Sharma suggest that combining the measurements of both methods allow the better understanding cloud distribution (Stefan et al., 2014).

In this work, we have focused on obtaining CBH from ground-based observation, meteorological simulation and, satellite-based approach, and compared the obtainable results from those three methods; ceilometer, SkewT/LogP diagram, and MODIS data. In addition, we intend to investigate cloud characteristics with the data obtained from the ceilometer.

Objectives of the research

1. To analyse the characteristics of CBH in the Northern of Thailand: CVS, the CBH distributions, and the distance between adjacent CBH.
2. To compare CBH obtaining from: Skew T/Log P diagram, ceilometer and MODIS.
3. To validate the obtained results by two statistical tests as mean bias deviation (MBD) and coefficient of determination (R-square: R^2)
4. To provide CBH database for being the resource of atmospheric research and application.

Significance of the research

Clouds strongly play an important role in the atmosphere, giving the study of cloud properties is then necessary, especially for CBH, for meteorology or aviation. Moreover, for rain making in royal project in Thailand, knowing the accurate CBH helps the pilots for more effective cloud seeding. To determine CBH and describe the effects of them to the Earth's atmosphere and others, there are three kind of measurements: ground-based, meteorological model simulation, and satellite-based measurements.

Scope of this work

Analysing the CBH over Omkoi, Chiang Mai, in the northern of Thailand, three approaches are used including ceilometer, SkewT/LogP diagram, and MODIS satellite. Moreover, we compare the CBH results from those three methods for validation and accuracy.

Research Hypotheses

1. CBH which is obtained from cloud simulation method: Skew T/Log P diagram and our ceilometer have good correlations.
2. CBH which is obtained from MODIS satellite and our ceilometer are validated and show similar trends.

List of abbreviations

| Abbreviation | Definition |
|--------------|---|
| CBH | cloud base height |
| CVS | cloud vertical structure |
| CVF | vertical frequency of cloud occurrence |
| CALIPSO | Cloud-Aerosol Lidar and Infrared Pathfinder Satellite Observation |
| MODIS | Moderate Resolution Imaging Spectroradiometer |
| RH | relative humidity |
| CCL | convective condensation level |
| LCL | lifting condensation level |
| NASA | National Aeronautics and Space Administration |
| NOAA | National Oceanic and Atmospheric Administration |
| LIDAR | light detection and ranging |
| CTH | cloud top height |
| CGT | cloud thickness |
| LWP | liquid water path |
| LWC | liquid water content |
| MBD | mean bias deviation |
| R^2 | coefficient of determination |

CHAPTER 2

Literatures review and theoretical background

This chapter will be divided into four sections; Earth's atmosphere, clouds, cloud observations and relevant research as follows.

1. Earth's atmosphere

The atmosphere is a cloud of gas and suspended solids. Earth's atmosphere extends more than 560 kilometers (348 miles) above the planet's surface, and is categorized into four layers according to the temperature and altitude, each of which has different characteristics and physical properties. (Ackerman & Knox, 2007; National Weather Service Shreveport, n.d.)

1.1 Troposphere

The troposphere is the lowest level beginning at about 4-12 miles (6-20 km) thus most all weather occurs in this layer. As the gases in this layer decrease with height, the air becomes thinner. Therefore, the temperature in the troposphere generally decreases with altitude. As you climb higher, the temperature drops from about 62°F (17°C) to -60°F (-51°C). The height of the troposphere varies from the equator to the poles. At the equator it is around 11-12 miles (18-20 km) high, at 50°N and 50°S, 5½ miles and at the poles just under four miles high. The transition boundary between the troposphere and the layer above is called the tropopause. It acts like a lid covering water from escaping.

1.2 Stratosphere

The Stratosphere extends from the tropopause up to 31 miles above the Earth's surface. This layer holds 19 percent of the atmosphere's gases but contains only a small amount of water vapor. Temperature increases with height as radiation is absorbed by oxygen molecules which leads to the formation of Ozone. The temperature

rises from an average -76°F (-60°C) at tropopause to a maximum of about 5°F (-15°C) at the stratopause due to this absorption of ultraviolet radiation. The increasing temperature causes it a calm layer with movements of the gases slow. The transition boundary which separates the stratosphere from the mesosphere is called the stratopause.

1.3 Mesosphere

Above the stratopause lies the mesosphere which extends from the stratopause to about 53 miles (85 km) above the earth. The gases, including the oxygen molecules, continue to become thinner with altitude. The effect of the warming by ultraviolet radiation becomes less, thus temperatures once again fall with increasing altitude, just as it does in the troposphere. On average, temperature decreases from about 5°F (-15°C) to as low as -184°F (-120°C) at the mesopause where separates the mesosphere from the thermosphere. However, the gases in the mesosphere are thick enough to slow down meteorites hurtling into the atmosphere, where they burn up, leaving fiery trails in the night sky.

1.4 Thermosphere

The Thermosphere extends from the mesopause to 430 miles (690 km) above the earth. This layer is known as the upper atmosphere. The gases of the thermosphere are increasingly thinner than in the mesosphere. Likewise, only the higher energy ultraviolet and x-ray radiation from the sun is absorbed. However, because of this absorption, the temperature again rises with height and can reach as high as $3,600^{\circ}\text{F}$ (2000°C) near the top of this layer. Although the high temperature, this layer of the atmosphere would still feel very cold to our skin because of the extremely thin air. The total amount of energy from the very few molecules in this layer is not sufficient enough to heat our skin.

From the mesosphere and thermosphere on up, the high-energy particles from the Sun become more influence to the atmosphere. These particles break apart

atmosphere molecules, which then form ions. For this reason, this region is sometimes called the ionosphere.

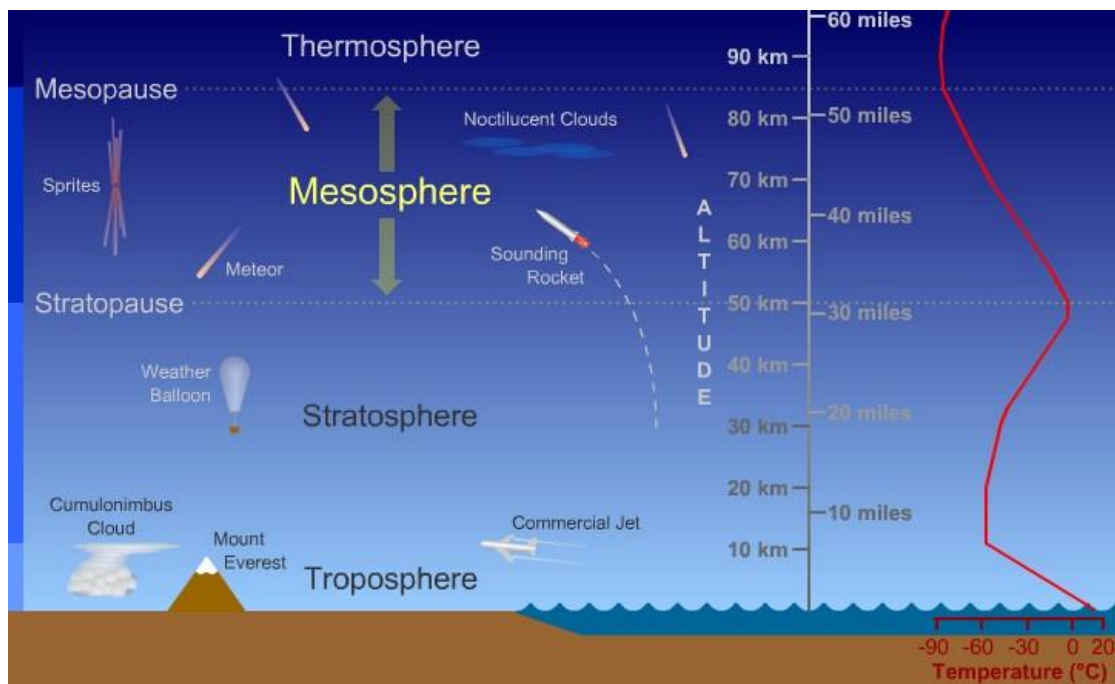


Figure 1. Structure of atmosphere (Russell, 2018)

2. Clouds

Clouds are made of water or ice in the air. Clouds are an important part of Earth's atmosphere. The properties of cloud, cloud formation, and cloud classification are explained in following these topics

2.1 Stable and unstable air

Temperature affects the Earth's surface and controls the buoyancy of air. It is also influence on cloud patterns, location and properties. Air temperature has alterable and uncommon pattern of change with height, unlike air pressure decreasing more rapidly. Temperature variations are given name into stability and instability air. Julian Mayers and Hughes defined that as follows: (Julian Mayers & Hughes, 2004)

2.1.1 Stable air

Stable air exists when a parcel of air is less buoyant than the surrounding air; vertical movement is discouraged unless the air is forced to rise (absolute stability). Consequently, cloud spread horizontally in a sheet-like pattern.

2.1.2 Unstable air

Unstable air occurs when a parcel of air is more buoyant than the surrounding air – including the air above (absolute instability); the lighter air tends to rise until a height is reached where all the air has the same degree of buoyancy. Accordingly, unstable air encourages vertical growth that result in a more sprase cloud distributions.

Table 1. The effect of stable and unstable air on cloud form

| Instability | Method and characteristic of uplift | Resulting cloud type |
|--------------|---|--|
| Stable air | Orographic uplift – slow Frontal uplift – Slow, widespread | Stratus family and related cloud types – horizontal development dominant |
| Unstable air | Convection – Rapid, often localized | Cumulus family – vertical development dominant |

2.2 Cloud formation

Condensation is a process whereby water-vapor molecules are caused to come together in sufficient numbers to produce liquid water. Understanding how condensation occurs, we need to consider the nature and temperature of the surface and temperature and relative humidity of the air. When the number of vapor molecules in the air increases the relative humidity also goes up. The air is saturated when the relative humidity reaches 100 per cent, thus it cannot contain any more moisture. At this point there is an equilibrium condition; the number of water-vapor molecules moving

from water to air exactly equals to the amount of water vapor in the air by measuring the pressure of the water vapor. As the air surrounding is cooled, the relative humidity is increased. Further cooling defines that the relative humidity is over 100 per cent, called super saturation. The supersaturated air means that there are more water vapor molecules than in stable saturated condition. We can calculate the relative humidity from,

$$R.H. = \frac{\text{Actual vapor pressure}}{\text{saturated vapor pressure}} \times 100 \quad (1)$$

The beginning of condensation occurs at dew point and the temperature of the air at that point is so called dew point temperature. Cloud droplets may form in condensation process, and cloud is also there.

Since the pressure is proportional to temperature. When an air mass moves up, it rises from higher pressure to the lower pressure. As the same, temperature also decreases with altitude. The term lapse rate determines temperature that reduces with altitude. The term adiabatic denotes process that no heat is gained or lost by the system. If the air is dry and no heat transfers to the system, it cools at rate of 1.0°C per 100 meters. This is the dry adiabatic lapse rate (Ackerman & Knox, 2007; Battan, 1962).

Hence, condensation starts when the air rises and temperature of the air decreases, and its relative humidity increases until reaches to the saturation. This is important principle for predicting the CBH which is the lowest level in the atmosphere. At that altitude, the air contains a perceptible quantity of cloud particles. (Bureau of meteorology, 2018)

2.3 Lifting processes that form clouds (Ackerman & Knox, 2007; Met office, 2018)

In general, most cloud formation occurs when the air cools to its dew point temperature as a parcel of air rises vertically. There are four mechanisms that cause air rising.

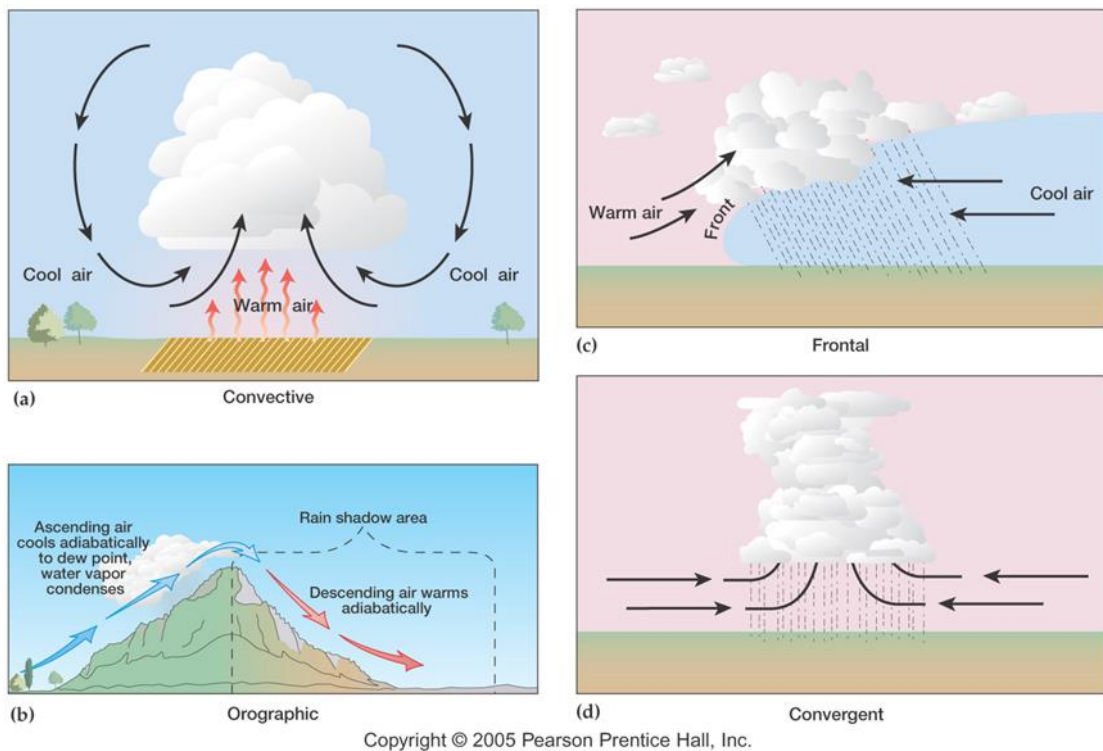


Figure 2. Four lifting processes that develop cloud (a) Convection, (b) Orographic lifting, (c) Frontal lifting, and (d) Convergence (Newman, 2006)

2.3.1 Convection

Convection is the process due to heat, it always occurs during summer. The less dense air near the surface warms and rises when solar energy passes through the atmosphere.

2.3.2 Orographic lifting

In airflow crossing against a hill, mountain or ridge, it cannot go through the mountain, it then flow over mountain. This is called orographic lifting. Orographic clouds may occur below, at or above the top of the obstacle.

2.3.3 Frontal lifting

“Front” means the boundary between two connecting air masses that are in different condition. Front is the significant term providing more understanding about

cloud formation and precipitation. Air masses do not mix easily when they meet up together. The less dense air mass will tend to move up over the other, creating a three-dimensional boundary called the frontal zone. Fronts are classified by temperature changes resulting after an air mass passes over a given location. The term warm front is used to describe a front that warm air replaces cold air on the earth's surface. In contrast, when cold air replaces warm air it is then called cold front. Occluded front is the complex front. Occlusion is formed when the cold front catches up the warm front.

Meteorologists often pinpoint the position of the cold front by blue line with triangles pointing the moving front way, and use red line for a warm front. As the same way, warm fronts have semi-circles pointing the way the front is moving. For Occluded front, the alternating triangles and semi-circles are used to denote this front.

(a)



(b)



(c)



(d)

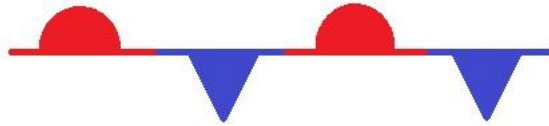


Figure 3. Weather front symbols (a) warm front, (b) cold front, (c) occluded front, and (d) stationary front

2.3.3.1 Cold front

Fronts develop in regions of lower pressure because air at the surface tends to blow toward lower pressure. This convergence of air helps intensify temperature and moisture contrasts, creating and sustaining fronts. After cold frontal passage the atmosphere pressure begins to increase as a cold, high pressure air mass moves into the region. The largest pressure changes usually occur in the frontal zone. On a cold front the cold polar air undercuts the warmer tropical air. This causes the ascent and cooling of air on the front resulting in thick cloud layers and precipitation. Some active cold fronts have occasional embedded cumulonimbus, and some are composed principally of convective cloud. Clouds become convective and well-broken behind front. A cold front can be an active feature with heavy rain and strong winds or weak with little or no rain.

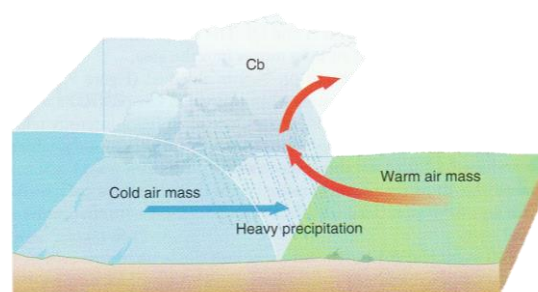


Figure 4. A cross section through cold front (Ackerman & Knox, 2007)

2.3.3.2 Warm front

A warm front occurs when the warm air replaces the cooler air. This upgliding warm air is a form of overrunning which occurs when an air mass moves over a colder and denser air mass. Deep layers of stratiform clouds (cirrostratus, altostratus, and nimbostratus) are often the result of overrunning. After the passage of a warm front, the air is warmer and often humid. As a warm front approaches, the temperature initially remains steady or climbs slowly and then rapidly increase during the frontal passage. The pressure drops as the warm front approaches and then increases as it passes by. Increasing amounts of upper cloud, thickening and lowering with approach of front.

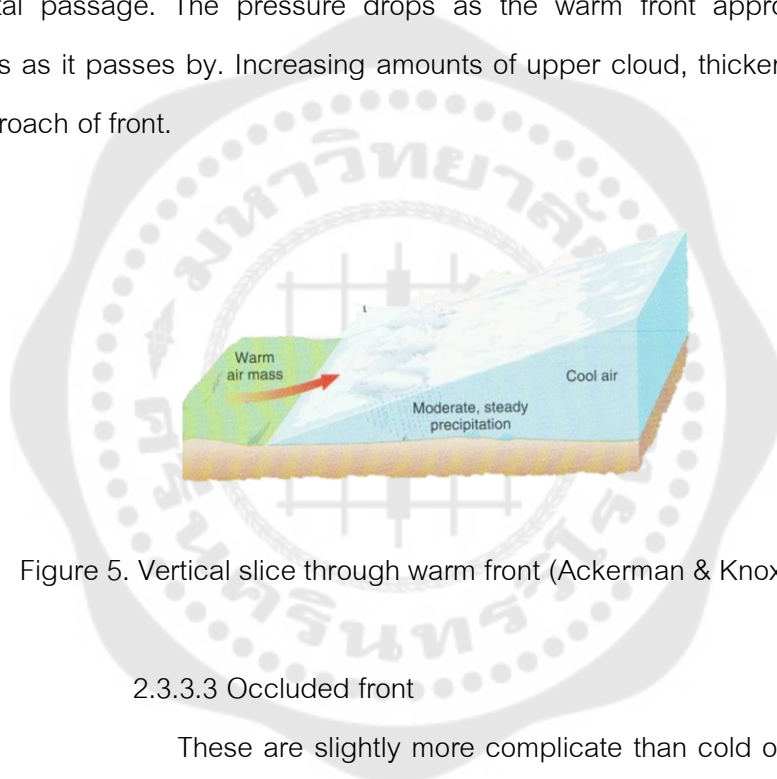
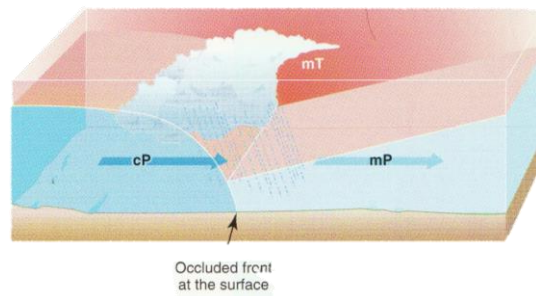


Figure 5. Vertical slice through warm front (Ackerman & Knox, 2007)

2.3.3.3 Occluded front

These are slightly more complicated than cold or warm fronts. An occlusion occurs when the cold front overtakes the warm front, the warm air is then lifted up from the surface. Whereas warm and cold fronts separate cold and warm air masses, an occluded front marks the surface boundary between two polar air masses. The warm air is aloft, lifted by its interaction with the polar air masses. The characteristics of both warm and cold front could have in an occlusion.

(a)



(b)

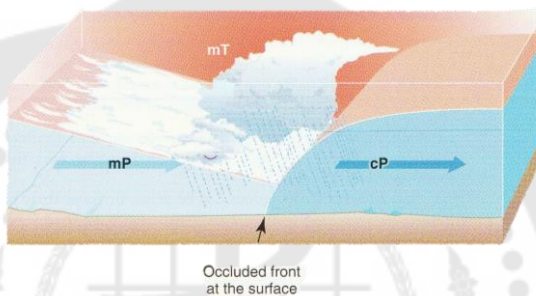


Figure 6. Occluded front (a) Cold-type occluded front, (b) Warm-type occluded front
(Ackerman & Knox, 2007)

2.3.3.4 Stationary front

Stationary front occurs when two air masses collide but move little or not at all at the surface. Although the front appears stationary at the surface, the air above can be moving causing overrunning. The warm air overrunning the colder air masses causes the clouds and precipitation along a stationary front.

2.3.4 Convergence

Convergence arises when air near the surface flows together from different directions. When the air near the ground converges, or is squashed together, it causes upward motion.

In each of these lifting processes, updraft is made up from the rising air. The updraft causes the cloud particles suspended in mid-air, although the gravity force drags them to the ground.

2.4 Cloud Composition (Ackerman & Knox, 2007; Bureau of meteorology, 2018)

The composition of each cloud is different, including phase of water in it, and shape and size of particles. Clouds over land tend to have a greater number of water droplets than cloud over the ocean. This is because of differences in water-bearing clouds. Continental clouds have about 500 million to 1 billion cloud droplets per cubic meter of air, while maritime clouds have some one tenth as many. But water content of both clouds is similar, so maritime clouds have large, soluble, and heterogeneous nuclei which favor the larger droplets formation.

The measured temperature of a cloud throughout its vertical extent will indicate its likely composition as either water droplets or ice crystals, or a combination of the two. Water droplets can be further classified as ordinary (or warm) water droplets, and supercooled water droplets; the latter being droplets colder than 0°C yet still in the liquid state.

The temperature at which the particles in a cloud will exist as ice crystals depends on a number of complex factors. A simple empirical rule suggests the temperature of -20°C (and colder) can be used as a guide to indicate the predominance of ice crystals within a cloud.

Table 2. The composition of each cloud type

| Cloud | Composition |
|------------------|---|
| Cirrus | Almost exclusively ice crystals. |
| Cirrocumulus | Almost exclusively ice crystals; strongly super-cooled water droplets may occur but are usually rapidly replaced by ice crystals. |
| Cirrostratus | Mainly ice crystals. |
| Alto cumulus | Almost invariably water droplets; when the temperature is very low, ice crystals may form. |
| Altostratus | <p>Water droplets and ice crystals. In the most complete case, three superposed parts may be distinguished:</p> <ul style="list-style-type: none"> • Upper part – wholly or mainly ice crystals • Middle part – mixture of super-cooled water droplets and ice crystals • Lower part – wholly or mainly ordinary or super-cooled water droplets. |
| Nimbostratus | As per Altostratus. |
| Stratocumulus | Water droplets; ice crystals may be present in extremely cold weather. |
| Stratus | Usually small water droplets; ice particles at low temperatures. |
| Cumulus | Mainly water droplets; ice crystals may form in those parts with a temperature well below 0°C. |
| Towering Cumulus | Water droplets and, especially in its upper portion, ice crystals; the water droplets may be substantially super-cooled. |

2.5 Types of cloud (Funk, n.d.; Julian Mayers & Hughes, 2004)

Clouds can be classified to many characters such as height above ground, appearance (texture), common cloud names, and kind of air movement. Summarizing of the following cloud roots and meaning:

| | |
|----------|---------------------|
| Cirro-: | high |
| Alto-: | mid |
| Strato-: | layer |
| Nimbo-: | rain, precipitation |
| Cumulo-: | heap |

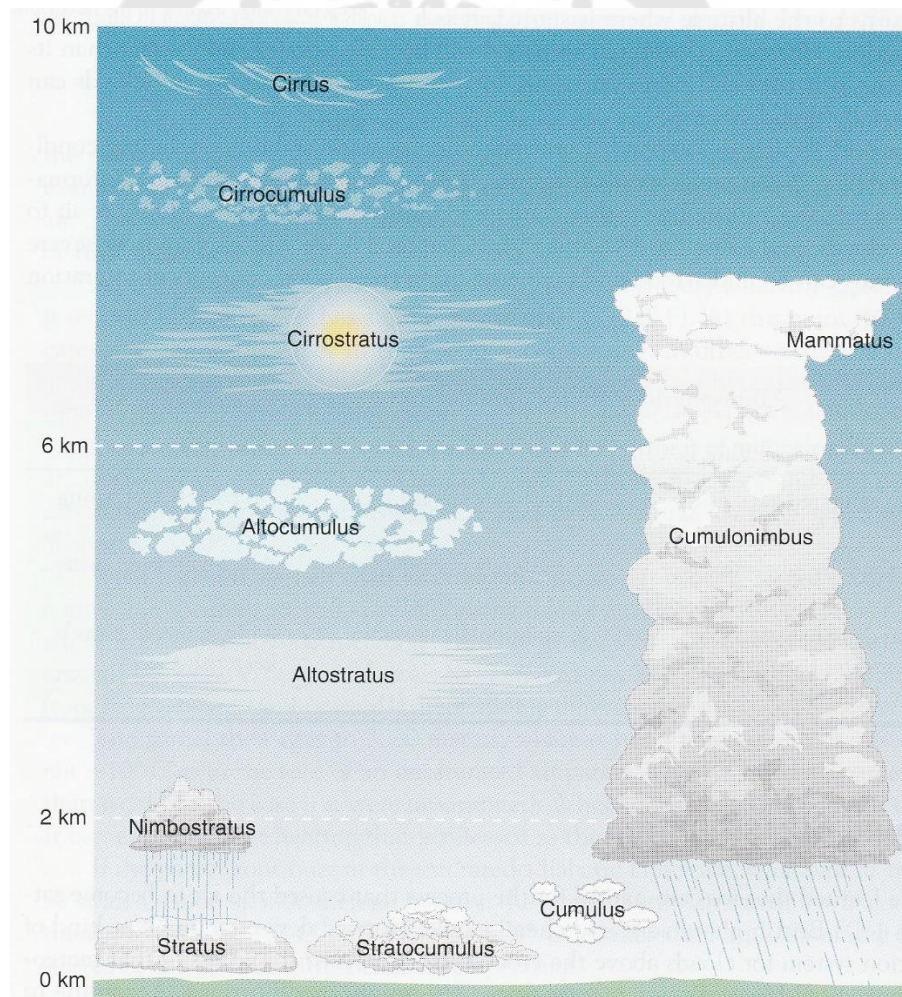


Figure 7. Type of clouds (Ackerman & Knox, 2007)

2.5.1 Based on level

One of the most popular data using in cloud classification is height above ground. The classification of cloud takes into account the CBH which is divided by following four groups.

2.5.1.1 High-level clouds

High-level clouds are at above over 20,000 feet and have the prefix “cirro-”. The atmosphere of this level is cold and dry, so the cloud compositions are ice crystals and often appear thin, streaky, and white (although a low sun angle, e.g., near sunset, can create an array of color on the clouds). The high cloud level has these main types: cirrus, cirrostratus and cirrocumulus.

1) Cirrus clouds are wispy, feathery, and have a hair-like appearance. They are composed entirely of ice crystals. They appear about 7 kilometers above. Cirrus clouds often are the first sign of an approaching warm front or upper-level jet streak.



Figure 8. Cirrus cloud (Schumacher, 2007)

2) Cirrostratus clouds are more widespread, veil-like layer. The sunlight or moonlight is dispersed or refracted when passes through ice crystal in the clouds, thus the halo could be formed.



Figure 9. Cirrostratus clouds (Mecelis, 2015)

3) Cirrocumulus clouds are layered clouds permeated with small cumuliform lumpiness. This cloud type combines the feature of cirrus with the globular pattern of cumulus. They also may line up in “streets” or rows of clouds across the sky denoting localized areas of ascent (cloud axes) and descent (cloud-free channels). It is hard to distinguish between this and altocumulus.



Figure 10. Cirrocumulus clouds (Everson, 2017)

2.5.1.2 Mid-level clouds

Mid-level clouds are composed of liquid water droplets, ice crystals, or a combination of the two, including super-cooled droplets. The middle cloud level occurs between 6,500 and 20,000 feet above the ground, and they are given the term “alto-” as prefix. The two main types of this cloud level are altostratus and altocumulus.

1) Altostratus clouds are flat and uniform appearance and white or grey colour. Altostratus clouds themselves do not produce significant precipitation at the surface, although sprinkles or occasionally light showers may occur from a thick altostratus deck.



Figure 11. Altostratus clouds (Gudd, 2016)

2) Altocumulus clouds like a cumulus blob spreading in the sky as a ripple. They may align in rows or streets of clouds, with cloud axes indicating localized areas of ascending, moist air, and clear zones between rows suggesting locally descending, drier air. Altocumulus clouds with some vertical extent may denote the presence of elevated instability, especially in the morning, which could become boundary-layer based and be released into deep convection during the afternoon or evening.



Figure 12. Altocumulus clouds (Omdal, 2016)

2.5.1.3 Low-level clouds

Low-level clouds have no prefix because it depends on their characteristics. Low-level clouds occur below 6500 feet. In general, their compositions are liquid water droplets or even super-cooled droplets, except during cold winter storms when ice crystals consist much of the clouds. The two main types of low clouds level are stratus and stratocumulus.

1) Stratus clouds are uniform and flat which develop horizontally at first 500 meters above. They create a grey layer covering cloud which may be precipitation-free or may cause periods of light precipitation or drizzle.



Figure 13. Stratus clouds (Knapp, 2014)

2) Stratocumulus clouds are mixtures of horizontal and vertical alignment, called stratus and cumulus, respectively. They typically occur between 500 and 2000 meters. Stratocumulus also can be thought of as a layer of cloud clumps with thick and thin areas. They occur frequently in the sky, either ahead of or behind a frontal system.



Figure 14. Stratocumulus clouds (Bruhn, 2006)

3) Nimbostratus clouds are thick, dense stratus or stratocumulus clouds producing steady rain or snow.



Figure 15. Nimbostratus clouds (Sugi, 2013)

2.5.1.4 Clouds with Vertical Development

1) Cumulus clouds have flat bottoms and round tops, and grow vertically. In fact, their name depends on the degree of vertical development. For instance, scattered cumulus clouds showing little vertical growth on an otherwise sunny day used to be termed "cumulus humilis" or "fair weather cumulus," although normally

they simply are referred to just as cumulus or flat cumulus. A cumulus cloud that exhibits significant vertical development (but is not yet a thunderstorm) is called cumulus congestus or towering cumulus.



Figure 16. Cumulus clouds (Linehan, 2010)

2) Cumulonimbus clouds are the developing cumulus cloud which has strong updrafts. They occur when the atmosphere has moisture. These clouds can produce lightning and thunder storms because of electrification many collisions between charged water droplets, graupel (ice-water mix), and ice crystal particles.



Figure 17. Cumulonimbus clouds (Favre, 2016)

There are other interesting clouds that are not classified in previous types.

Wall Cloud: A localized lowering from the rain-free base of a strong thunderstorm. The lowering denotes a storm's updraft where rapidly rising air causes lower pressure just below the main updraft, which enhances condensation and cloud formation just under the primary cloud base. Wall clouds take on many shapes and sizes. Some exhibit strong upward motion and cyclonic rotation, leading to tornado formation, while others do not rotate and essentially are harmless.



Figure 18. Wall cloud (Penry, 2013)

Shelf Cloud: A low, horizontal, sometimes wedge-shaped cloud associated with the leading edge of a thunderstorm's outflow or gust front and potentially strong winds. Although often appearing ominous, shelf clouds normally do not produce tornadoes.



Figure 19. Shelf cloud (Thompson et al., 2013)

Fractus: Clouds in low, ragged stratiform or cumuliform cloud elements that normally are unattached to larger thunderstorm or cold frontal cloud bases. Also known as scud, fractus clouds can look ominous, but by themselves are not dangerous.

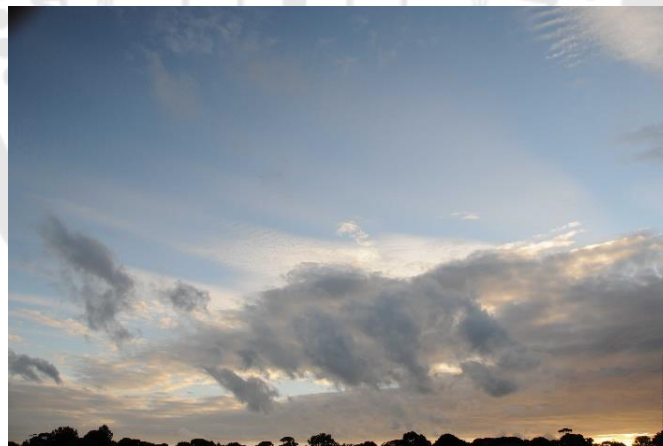


Figure 20. Fractus (Bruhn, 2010)

Mammatus: Drooping underside (pouch-like appearance) of a cumulonimbus cloud in its latter stage of development. Mammatus most often are seen hanging from the anvil of a severe thunderstorm, but do not produce severe weather. They can accompany non-severe storms as well.



Figure 21. Mammatus (Dorr, 2018)

Contrail: Narrow, elongated cloud formed as jet aircraft exhaust condenses in cold air at high altitudes, indicative of upper level humidity and wind drift.



Figure 22. Contrail (Theberge, 2018)

Fog: Layer of stratus clouds on or near the ground. Different types include radiation fog (forms overnight and burns off in the morning) and advection fog.



Figure 23. Fog (Schwemmer, 2013)

2.5.1 Based on appearance (Moran & Mogan, 1997)

Stratiform clouds are layer clouds and spread laterally. These clouds are developed by gentle updraft of air (typically less than 5 centimeters/second or 1.0 miles/hour) over broad sky.

Cumuliform clouds are heaped or puffy in appearance. These clouds grow in vertical and cover smaller areas. Cumuliform clouds are associated with much more strong updraft (sometimes in excess of 30 centimeters/second or 70 miles/hour).

2.6 Atmospheric scattering (Nave, n.d.)

Scattering is the process that the particles change the direction when they collide with another particles. As atmospheric scattering, sunlight passes through the atmosphere and is scattered by the aerosols or droplets in a medium. There are three types of scattering: Rayleigh scattering, Mie scattering, and Raman scattering.

2.6.1 Rayleigh scattering

Rayleigh scattering is a kind of an elastic scattering for the energy of photon is not changed. It occurs when the wavelength of light greater than the size of particle causing scattering, also called depending on wavelength. This kind of scattering causes blue sky appearing because Rayleigh scattering is more effective at short wavelength (blue range).

2.6.2 Mie scattering

Mie scattering is an elastic scattering as Rayleigh scattering. It is not wavelength dependent, and occurs when the light wavelength smaller than the size of particle causing scattering, such as dust, pollen, or water droplets. Because of Mie scattering, the clouds appear white.

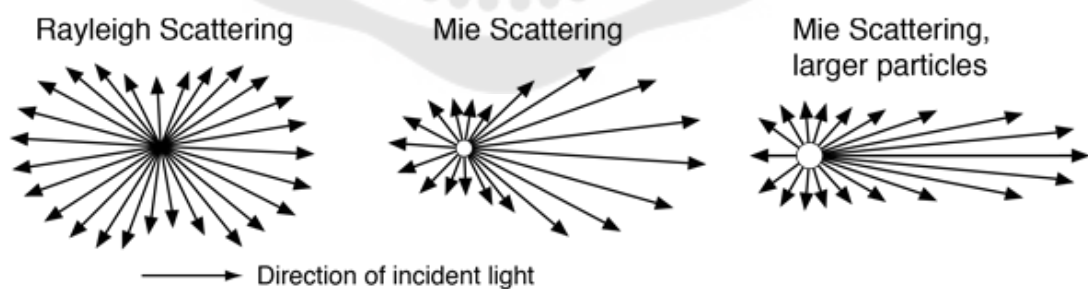


Figure 24. The difference of Rayleigh scattering and Mie scattering (Nave, n.d.)

2.6.3 Raman scattering

Raman scattering is an inelastic scattering since the photon energy not be the same. This involves exciting some vibrational mode of the molecules.

The repeated scattering of light is called multiple scattering. It creates whitish light since all clours of light is scattered to our eyes. Clouds appear white because of this scattering, and scattered light by clouds is also important in climate change. Clouds are responsible for radiation budget which dues to multiple scattering in clouds. In the other words, if the average particle size of clouds became smaller, the cloud would be brighter and more solar energy would be lost from the atmosphere. (Ackerman & Knox, 2007)

3. Cloud observations

Bureau of meteorology training centre explains the description cloud observations that they consist of identifying the types of clouds present, estimation of the amount of each cloud type, and estimation of the height of the cloud base for each cloud type (Bureau of meteorology, 2018).

3.1 Cloud amount observation

The total cloud cover is the fraction of the celestial dome covered by all the clouds observed. The term cloud amount in reference to a genus, a species, a variety, a layer, or a certain combination of clouds indicates the fraction of the sky cover by that terms. This fraction is represented by a figure equivalent to how many eighths or oktas of the sky is covered.

Table 3. The estimation of cloud amounts

| Oktas | Description |
|-------|--|
| 0 | sky completely clear |
| 1 | from a trace of cloud up to 1/8 |
| 2 | more than 1/8 but not more than 2/8 |
| 3 | more than 2/8 but not more than 3/8 |
| 4 | more than 3/8 but not more than 4/8 |
| 5 | more than 4/8 but not more than 5/8 |
| 6 | more than 5/8 but not more than 6/8 |
| 7 | more than 6/8 but not total coverage i.e. if there is any sky visible then use 7/8 |
| 8 | sky completely overcast (no breaks or openings) |

Importantly, cloud amounts are generally round up to the next okta. For example 2 and a bit oktas is rounded to 3 oktas. In the other hand, there exception for cloud amounts when more than 7 but not reach 8 oktas, for this example cloud amount is rounded down to 7 oktas.

3.2 CBH observation

The cloud base is the lowest area in which the obscuration corresponding to a change from clear air or haze to water droplets or ice crystals cause a significant change in the profile of the backscatter extinction coefficient or more simply, the lowest level in the atmosphere where the air contains a perceptible quantity of cloud particles.

The CBH is always expressed in terms of the height above the station level. For all reporting and broadcast mechanisms, the unit used to express the height of

cloud is feet. For example, when clouds are observed over distant hills, the cloud base may be only 500 feet above the tops of the hills, but if the tops of the hills are 2000 feet above the station level, then the cloud base is reported at 2500 feet.

3.3 CBH observation methods

There are three difference types of CBH observation using in this work, ground-based, cloud simulation, and sky-based observation.

3.3.1 Radiosonde

Radiosonde measurement is the most accurate information available for understanding weather. A radiosonde is radio-equipped instrument package carried aloft by a weather balloon. The instrument transmits to a ground station vertical profiles of air temperature, pressure, and relative humidity up to an altitude of about 30 kilometers. They can estimate how weather will change in the next few hours. The vertical profiles of air temperature, RH, and pressure can be detected by radiosonde (Moran & Mogan, 1997; Vaisala, 2016).

3.3.2 SkewT/LogP Diagram (AIR WEATHER SERVICE SCOTT AFB IL., 1990; Mcmurdie, 2007)

The SkewT/LogP Diagram shows the relationships of physical data, for instances, isobar, isotherm, dry adiabats, dew point temperature, and saturation mixing ratio. The SkewT/LogP Diagram was developed from the Emagram by skewing the isotherm to nearly 45 degrees from the vertical to increase the angle between isotherms and adiabats. This plot is commonly called a sounding which sounding data come from weather balloons. SkewT/LogP Diagram is generally used in meteorology for weather forecast and aviation. In this section, we focus on reading CBH, so these following section are the diagram description and plotting the data for CBH prediction.

Isobar are horizontal and solid lines spaced logarithmically for 10-mb intervals.

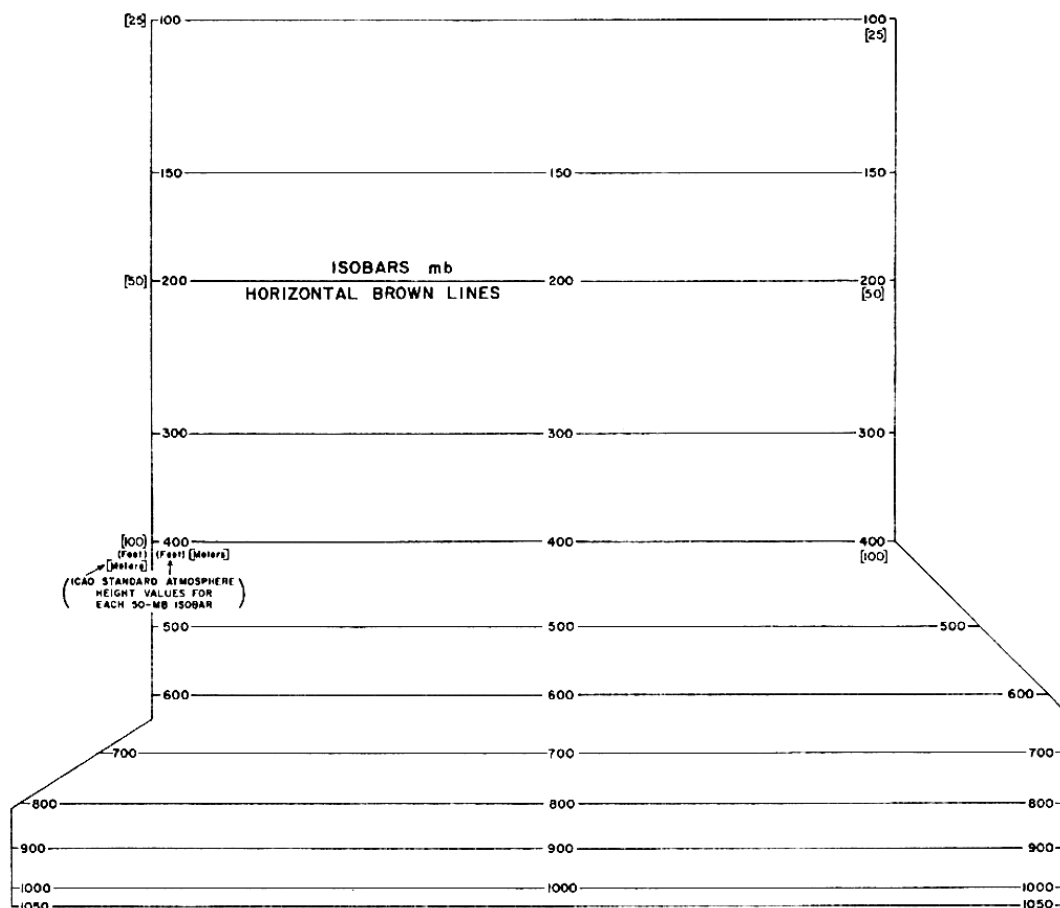


Figure 25. Isobars on SkewT/LogP diagram.

Isotherm are straight and solid lines, slopping from the lower left to upper right. This line have an equal range over entire diagram.

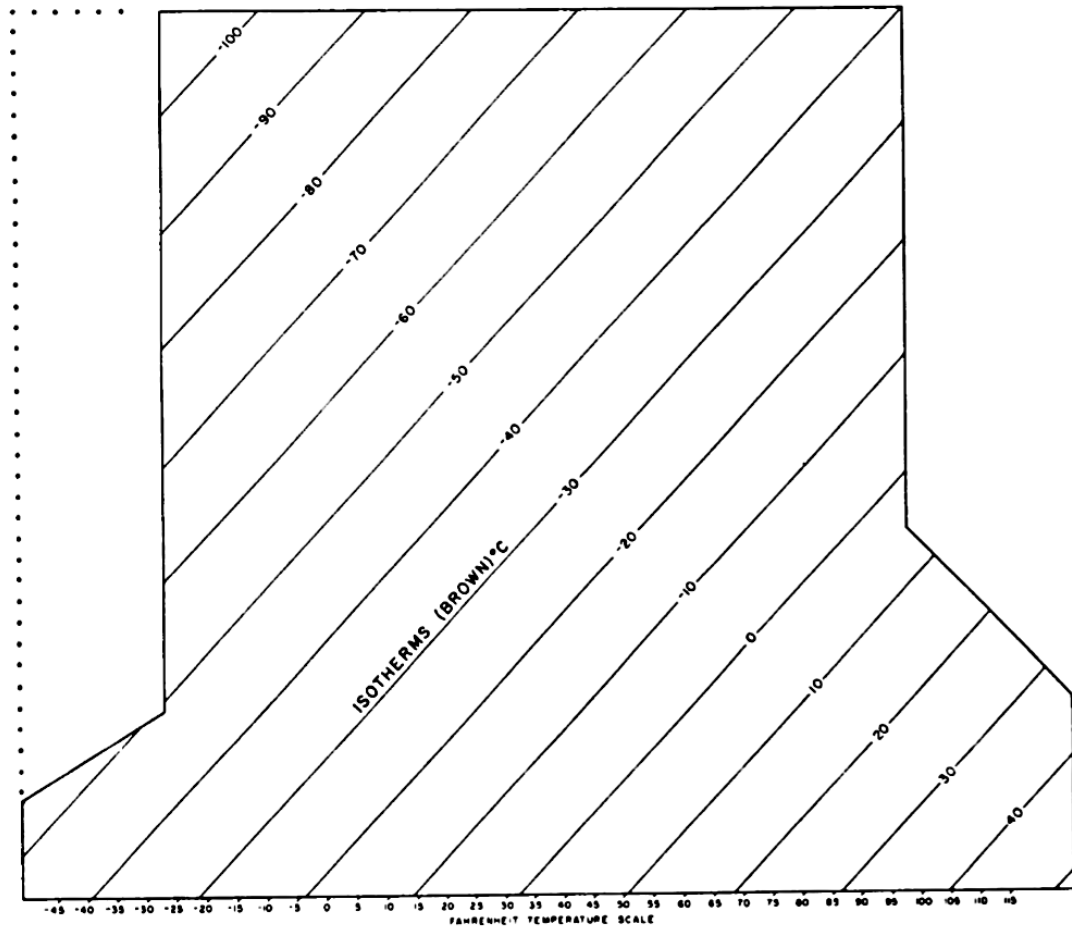


Figure 26. Isotherms on SkewT/LogP diagram

Dry Adiabats are the slightly-curved and solid lines slopping from the lower right to upper left. They indicate the rate of temperature change in a parcel of dry air rising adiabatically.

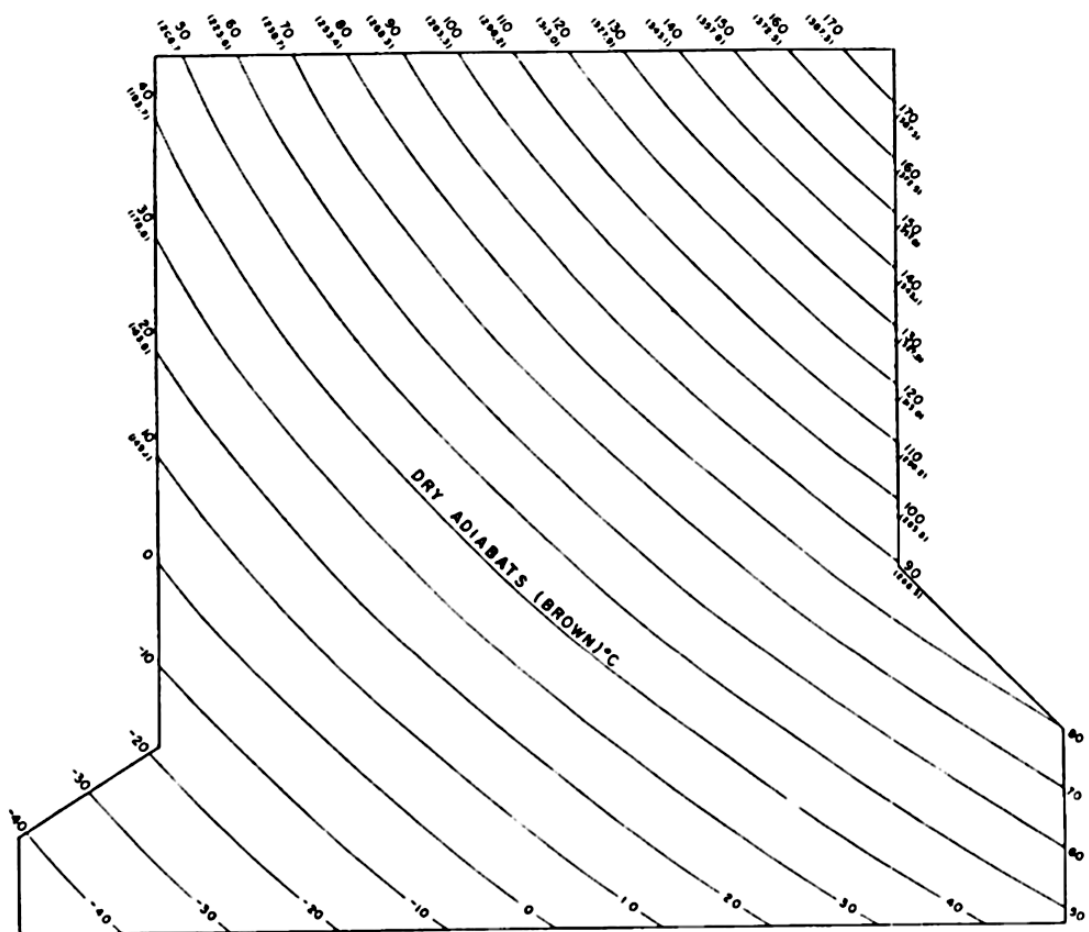


Figure 27. Dry adiabats on SkewT/LogP diagram

Saturation mixing ratio is the mixing ratio of a saturated parcel of air, where the mixing ratio is the ratio of the mass of water vapor in the air over the mass of dry air. They are labeled in parts of water vapor per 1000 parts of dry air (labeled in grams/kilogram). Saturation mixing ratio depends on temperature, higher temperature, greater saturation mixing ratio. This line is slightly curved, dashed, sloping from lower left to upper right.

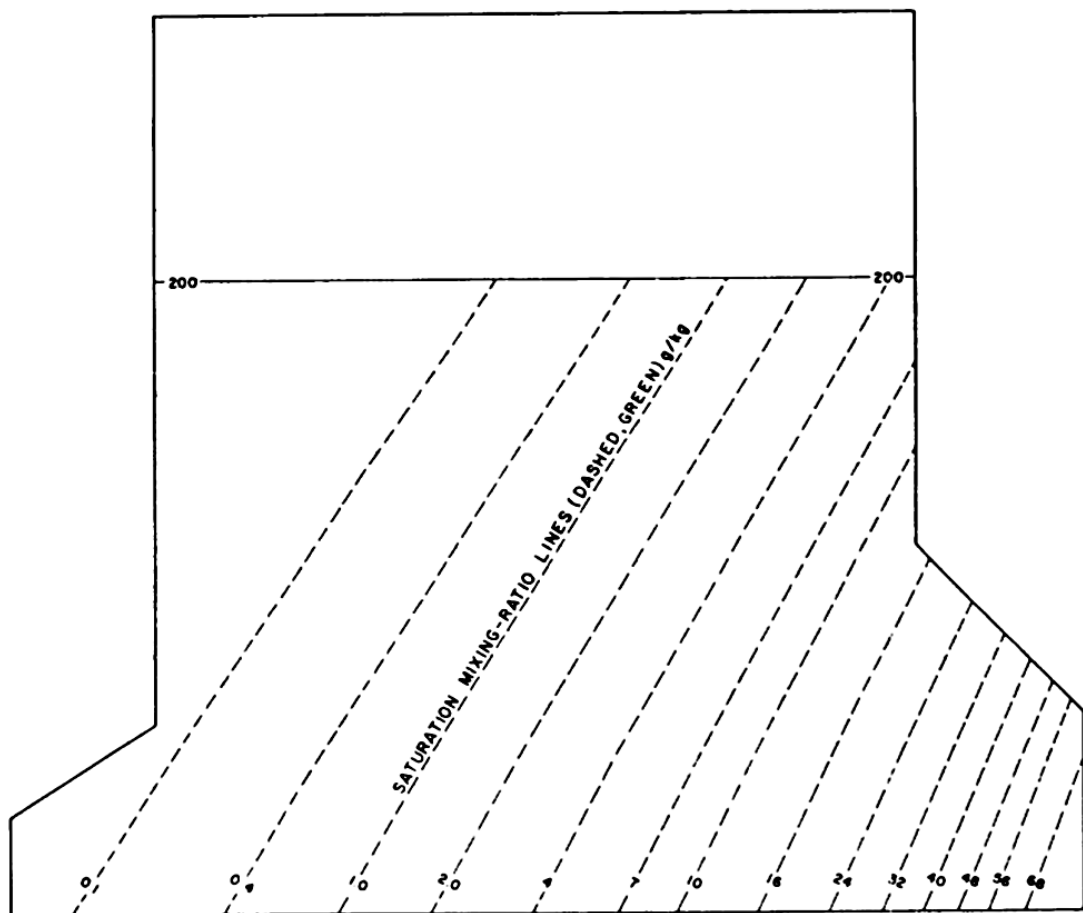


Figure 28. Saturation mixing ratio on SkewT/LogP diagram

Convective condensation level (CCL) is the altitude at which condensation begins to occur through thermal convection. This level is decided to be a base of cloud.

Procedure: From the surface dew-point temperature, draw a line along the saturation mixing ratio line to where it intersects the environmental temperature curve. The position where these two lines intersect is the CCL.

Lifting condensation level (LCL) is the altitude at which the parcel of air becomes saturated when it is lifted dry adiabatically. This level also conforms to the cloud base. The LCL for a surface parcel is always found at or below the CCL.

Procedure:

1. From the dew-point temperature of the level for which the LCL is required to be determined, draw a line upward parallel to the saturation mixing ratio lines.
2. From the temperature value of the level in which the LCL is required, draw a line upward parallel to the dry adiabat lines. The position where these two lines intersect is the LCL.

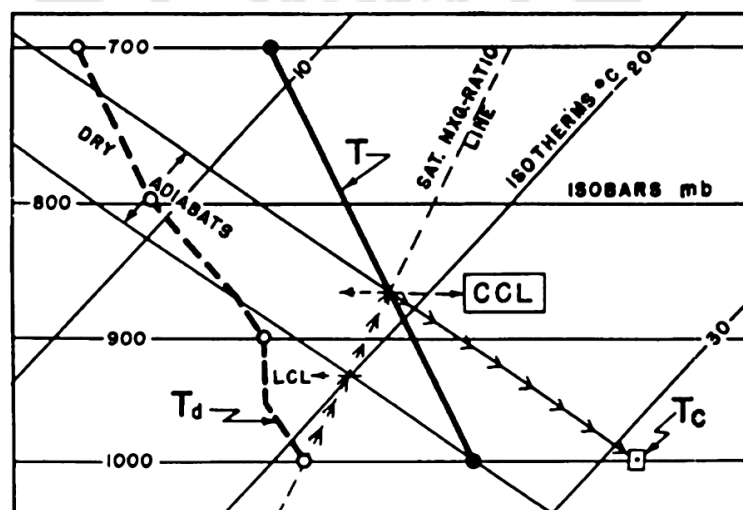


Figure 29. CCL and LCL on SkewT/LogP diagram (Ceilometers Net, 2015)

3.3.3 Ceilometer

The ceilometer is launched for detecting and measuring cloud height, sky condition, raw backscatter profiles, and vertical visibility for meteorological and aviation applications. Calculations of the backscattered signal $P(H)$ are similar to the analysis of conventional lidar, can be written in the form (K. Holejko & Nowak, 2000).

$$P(H) = A_0 a(h_b) \int_0^H P_0(t) \frac{\beta(\pi)}{(h_b + h)^2} e^{-2\alpha h} dh \quad (2)$$

where A_0 is aperture of receiving telescope, h is the distance in the cloud ranging from the cloud base h_b to the determined point of the cloud H ; $(H = h_b + h)$, $a(h_b)$ is the atmospheric transmittance up to the cloud base, $P(t)$ is the laser beam power, α is the total extinction coefficient of the cloud, and $\beta(\pi)$ is the backscattering coefficient. The term t is time derived from $\frac{2H}{c}$, where 2 shows forth and back pulse paths.

To obtain the CBH, ceilometer will emit laser pulse through the atmosphere. When this light pulse is scattered by aerosol particles, it then be received back by the receiver.

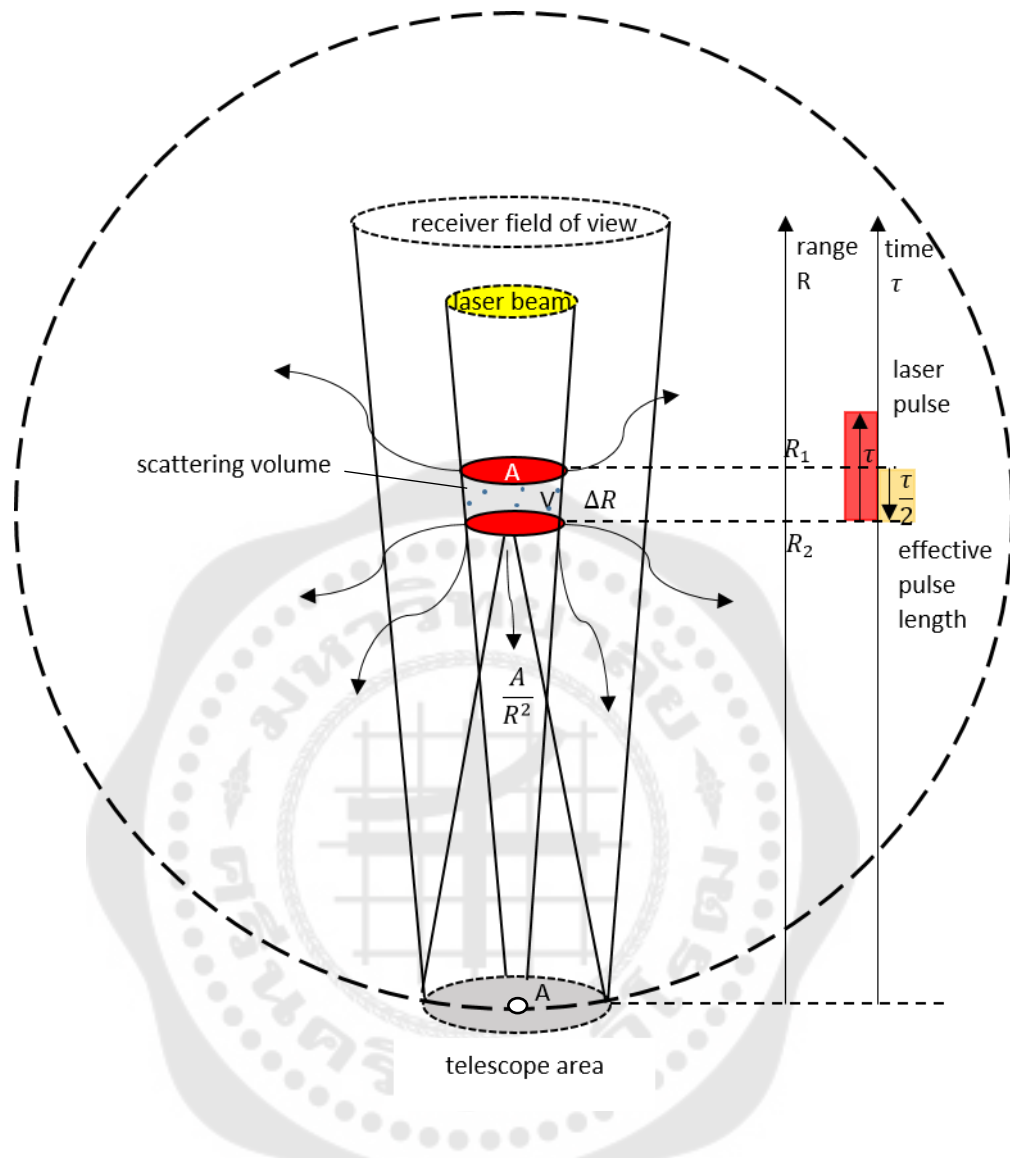


Figure 30. Ceilometer single lens overlap geometry modified from (Ceilometers Net, 2015)

3.3.4 MODIS satellite

Moderate Resolution Imaging Spectroradiometer (MODIS) is a passive remote sensor and launched into the Earth's orbit with two satellite: Terra and Aqua by National Aeronautics and Space Administration (NASA). There is a schedule of Terra's orbit and Aqua's orbit around the Earth that Terra passes from north to south across the equator in the morning, while Aqua passes south to north over the equator in the afternoon. MODIS can sweep 2,330 kilometers wide viewing swath in every 1-2 days.

MODIS provide 36 discrete spectral bands which can measure the properties of clouds and aerosols. MODIS provide information about global dynamics and processes occurring on the land, in the oceans, and in the lower atmosphere. (NASA, n.d.)

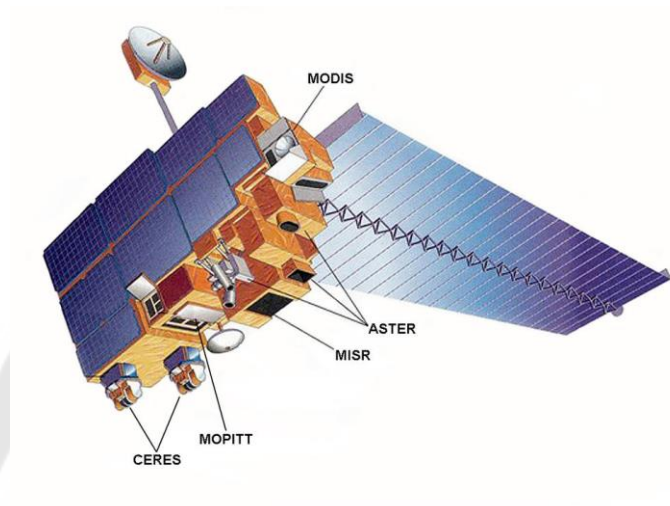


Figure 31. Terra spacecraft (NASA, 2017)



Figure 32. Aqua spacecraft (NASA, 2018)

4. Relevant research

Costa-Surós studied cloud occurrence, cloud vertical structure, cloud base height distributions, and CBH behavior during some season situation observed by ceilometer. This work covered four years (2007-2010) at Girona, Spain. The significant differences of two seasons; winter and summer, are shown involving specific conditions (Costa-Surós et al., 2013).

Sharma studied the CBH by using ceilometer during 2013-2015 over the western area in India and compared with the Moderate Resolution Imaging Spectroradiometer (MODIS) satellite. The observed CBH by ground-based measurement and satellite measurement were shown in fine correlation over that area. They also presented cloud characteristic in different periods of monsoon and post-monsoon, respectively (Sharma et al., 2016).

Rui and Abel presented a real-time cloud simulation method based on SkewT/LogP diagrams. Their cloud simulator system was based on physics concept without solving differential equations of cloud motion to achieve real-time rates. Their work was widely used for simulator in some industries, namely movies, virtual environments, and video games. They simulated 3D clouds from sounding data which have been published worldwide by weather agencies for being atmospheric database (Rui P.M. Duarte & Abel J.P. Gomes, 2017).

Peengam investigated CBH and cloud cover in tropical site in northern Thailand by ceilometer CS135. The results showed that CBH varied all the times and more variations were found in rainy day. Most of clouds classified were low-level clouds. They compared the outcome from ceilometer between LIDAR of MPLNET and MODIS satellite, however, the results from both method were in reasonable agreement and obviously different, respectively. For cloud cover results, they found variation in the morning until evening depending on the seasons (Peengam, 2017).

Lee investigated CBH and vertical frequency of cloud occurrence obtained by ceilometer in Seoul metropolitan site, Korea, during three years (2014-2016). A monthly variation of vertical frequency of cloud occurrence revealed that frequency

concentration of lower clouds was found in summer and winter, and higher clouds more often detected in spring and autumn. Also, the diurnal and daily variations of CBH and vertical frequency of cloud occurrence were represented (Lee et al., 2018).



CHAPTER 3

Research methodology

This chapter describes the methodology that uses in this study for analysing CBH from three methods including ceilometer, SkewT/LogP diagram, and MODIS satellite.

1. Framework

The process of CBH analysis is illustrated in Fig. 33.

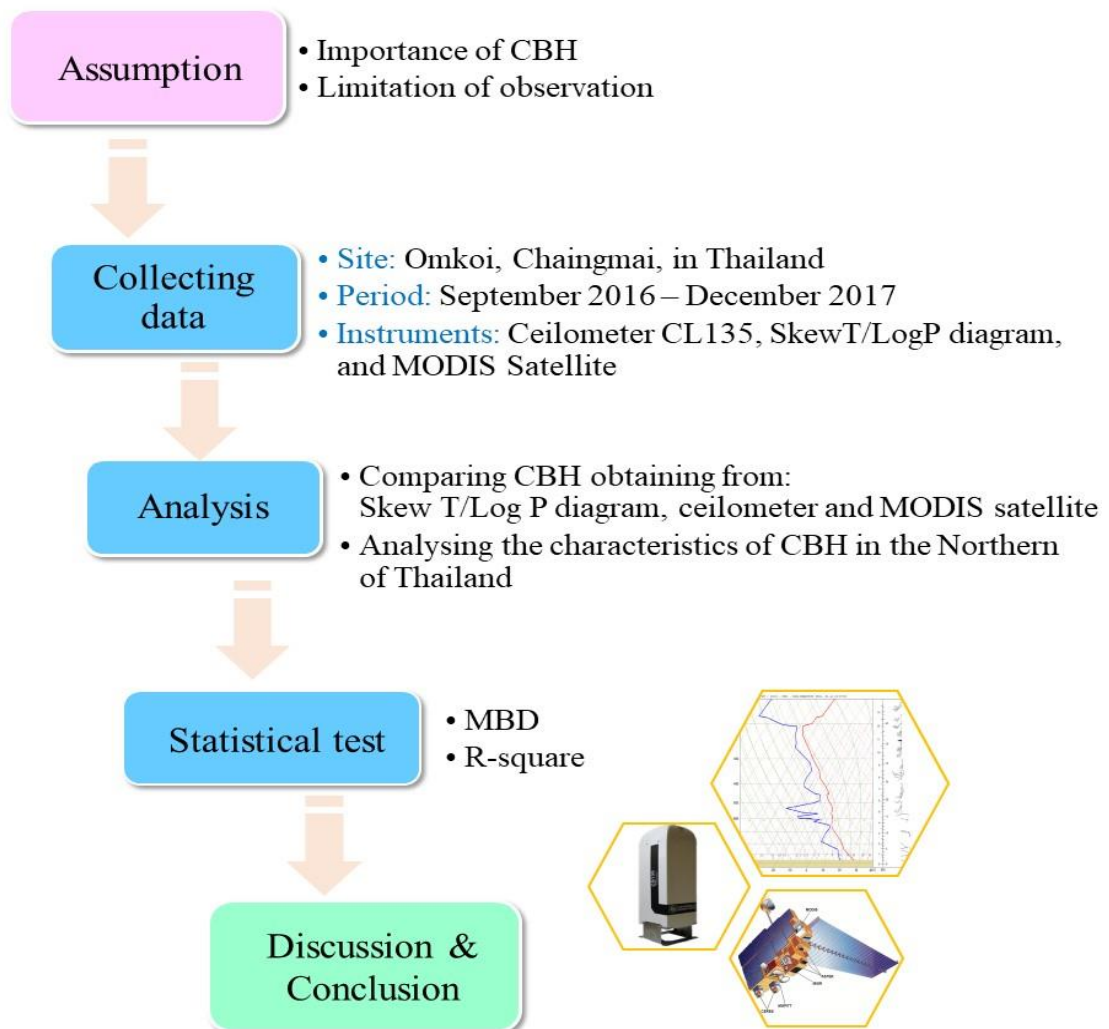


Figure 33. Research framework

2. Research methods

In this work, we detect and determine CBH by using ceilometer, SkewT/LogP diagram and MODIS satellite which are ground-based measurement, meteorological model simulation, and sky-based observation, respectively.

2.1 Ceilometer

Ceilometer is set up at Omkoi, Chiang Mai province in the Northern of Thailand by Sipakon University. Ceilometer uses LIDAR (light detection and ranging) technology, and consists of vertically pointing laser and receiver at the same location. It employs pulsed diode laser InGaAs (Indium Gallium arsenide) and operates a wavelength of 912 nm (± 5 nm). It can provide the information of cloud up to consecutive four layers. In this study, we use CS135 LIDAR Ceilometer from the Operation of a Campbell Scientific. The technical specification of ceilometer CS135 is shown in table 4.

Table 4. Technical specification of ceilometer CS135.

| Properties | Description / value |
|-----------------------|---|
| Reporting range | 0 to 10 km (0 to 32,808.4 feet) |
| Laser source | Indium gallium arsenide (InGaAs) class 1M |
| Reporting cycle | 15 seconds |
| Laser wavelength | 912 nm (± 5 nm) |
| Cloud layers reported | Up to four layers |

The output data is sent to Viewpoint software, a graphical display program, connecting to personal computer or laptop. However, we have to collect and analyse backscattered profile by Campbell Scientific data logger CR1000 which records every five minutes. The display of Viewpoint software and the feature of ceilometer CS 135 are shown in Fig. 34 and Fig. 35, respectively.

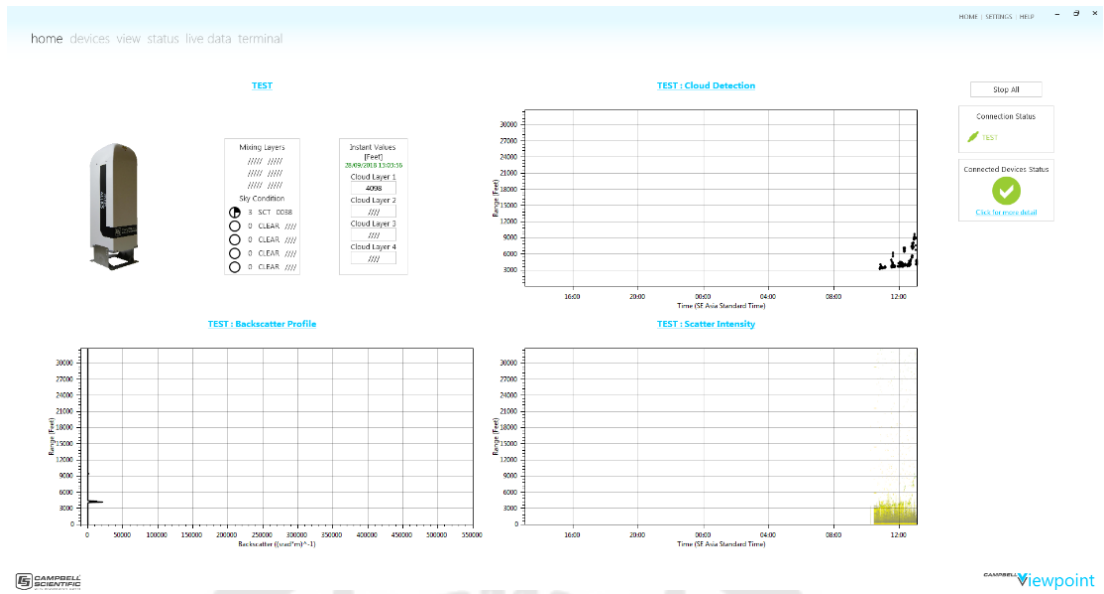


Figure 34. Display of Viewpoint software



Figure 35. Campbell Scientific ceilometer CS135 (Campbell scientific, 2018)

2.2 SkewT/LogP diagram

We obtain the SkewT/LogP chart and data from Department of Royal Rainmaking and Agricultural Aviation website (<http://www.royalrain.go.th>) which are open source and available online, shown in Fig. 36. An atmospheric sounding is a set of raw data received by radiosonde balloon at different pressure. As a balloon moving upward in the atmosphere, the vertical motion of a cloud in the atmosphere is described. The obtained data including temperature profile and other atmospheric data

allow us to determine the CBH. Plotting this diagram, an atmospheric sounding are used.

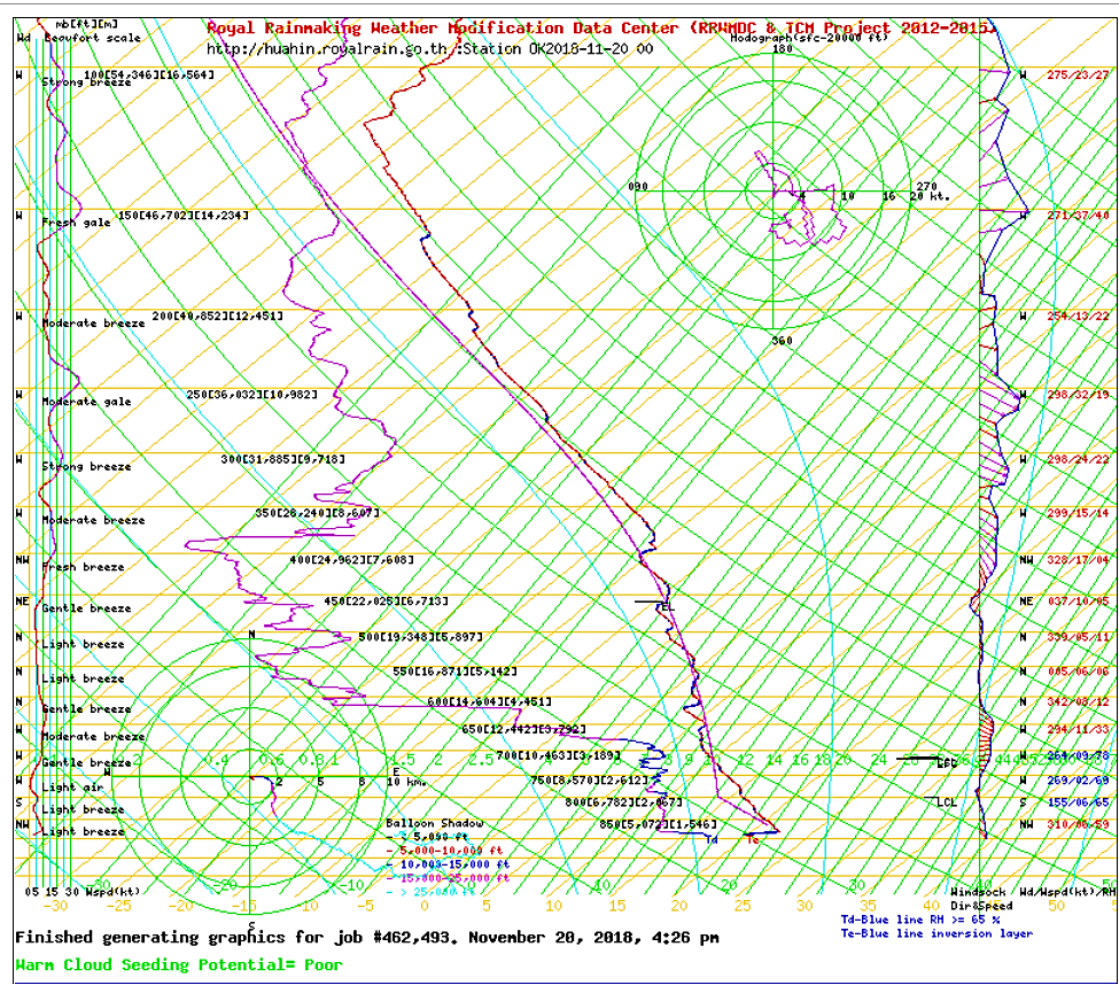


Figure 36. Display of SkewT/LogP diagram from Department of Royal Rainmaking and Agricultural Aviation website

2.3 MODIS Satellite

The MODIS cloud product employs infrared and visible range to determine both physical and radiative cloud properties such as cloud-particle phase, effective cloud-particle radius, and cloud optical thickness. There are two MODIS cloud data product files stored in HDF format: MOD06_L2, containing data collected from the Terra platform; and MYD06_L2, containing data collected from the Aqua platform. These data

are available online in <https://ladsweb.modaps.eosdis.nasa.gov/>. MODIS passes through Thailand every 1-2 times a day and provides only CTH data, so we have to use algorithm for CBH determination.

Sharma revealed this algorithm as follows (Sharma et al., 2016),

$$CBH = CTH - CGT \quad (3)$$

$$CGT = \frac{LWP}{LWC} \quad (4)$$

where CTH is cloud top height (m)
 CGT is cloud thickness (m)
 LWP is liquid water path (gm^{-2})
 LWC is liquid water content (gm^{-3})

The value of LWC varies in some range according to the cloud types and environment which is shown in table 5.

Table 5. The liquid water content of the cloud in each cloud types (Linacre & Geerts, n.d.)

| environment | Cloud type | LWC |
|-------------|----------------------------|-----------|
| Continental | Stratus | 0.28 |
| | Cumulus (clean) | 0.26 |
| | Cumulus (polluted) | 0.3 |
| | Cumulonimbus (growing) | 1-3 |
| | Cumulonimbus (dissipating) | 1.0 - 1.5 |
| | fog | 0.06 |

| environment | Cloud type | LWC |
|-------------------------|------------------|-------|
| maritime | stratus | 0.30 |
| | (strato) cumulus | 0.44 |
| Continental or maritime | Cirrus (-25°C) | 0.03 |
| | Cirrus (-50°C) | 0.002 |

This algorithm is limited to daytime only, because LWP is available only in sunlit regions.

3. Research Site and Data collection

3.1 Research Site

Ceilometer CS135 is launched at Radar station of Department of Royal Rainmaking and Agricultural Aviation which is located at Omkoi district, Chiang Mai province in northern of Thailand (17.79°N, 98.43°E). Omkoi is on average at 1,120 feet elevation. There are enormous forests and mountains covering this area. Omkoi's climate is classified as tropical. The average annual temperature is 28.4°C, and precipitation is 1173 mm. (Climate data, n.d.; Peengam, 2017)

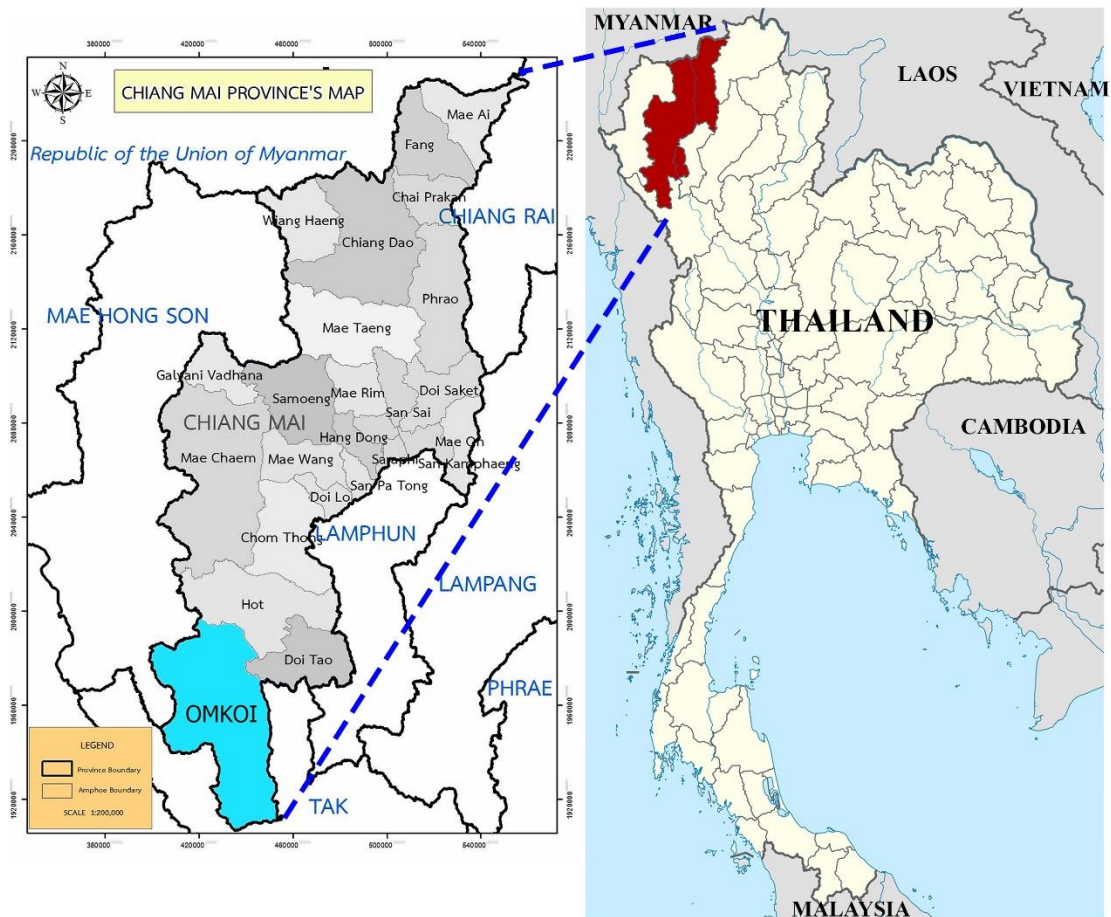


Figure 37. The location of Chiang Mai province, Northern of Thailand modified from (NordNordWest, 2009; Orange Smile, n.d.)

3.2 Data collection

We collect height of cloud base data from September 2016 to December 2017. From the total possible measurements during this period, these three months: May 2017 to June 2017 were absent because the ceilometer was in maintenance.

4. Data analysis

To analyse the characteristics of cloud and understanding cloud distribution, we consider these following topics which is obtained from ceilometer.

4.1 Cloud vertical structure (CVS)

Ceilometer measurements allow retrieving information on the vertical structure of the cloud, although CTH cannot be detected directly. Ceilometer can perform a measurement up to consecutive four layers of clouds, resulting the possible study of CVS and frequency of cloud occurrence.

4.2 The CBH distributions

CBH distributions retrieved from the ceilometer are shown in this section in order to better comparing cloud shapes and showing their characteristics in each seasons. Also, compared the single day variation with the sky image captured by sky view camera

4.3 The distance between adjacent CBH

For multilayered cloud aggregation, distances between consecutive layers of CBH are analyzed to examine cloud characteristics.

4.4 Comparison of CBH obtained from ceilometer and SkewT/LogP diagram

SkewT/LogP diagram is able to demonstrate the theoretical CBH value and predict the cloud base occurrence, while the ceilometer provides a real time CBH information. Therefore, we compare the performance of these two methods for the validation and accuracy including, two statistical tests. Furthermore, comparing both method helps the pilot more effective rainmaking. When they know more precise CBH, cloud seeding are more capable.

4.5 Comparison of CBH obtained from ceilometer and MODIS

Ceilometer is lied near the passing satellite so that they are used in comparison propose. To evaluate the performance of ground based measurement and satellite based measurement, ceilometer and MODIS are the representation of that kind of observation, respectively.

5. Statistic validation

To validate the CBH results obtaining from three observation methods: SkewT/LogP diagram, ceilometer and MODIS satellite, we use these two following statistical tests including mean bias deviation (MBD) and coefficient of determination (R-square: R^2). (Pukdeekiat, 2016; Vongpadai, 2016)

5.1 Comparison of CBH obtained from ceilometer and SkewT/LogP diagram

5.1.1 Mean bias deviation (MBD)

MBD shows the deviation or difference between expected and measured value. The most accurate model has an MBD value closed to zero. Generally, MBD can give negative and positive value; a negative value means that the model underestimates, while a positive value means the model overestimate.

$$MBD = \frac{\sum_{i=1}^N (CBH_{ceilometer} - CBH_{SkewT/LogP})}{\frac{\sum_{i=1}^N CBH_{SkewT/LogP}}{N}} \times 100\% \quad (5)$$

where $CBH_{SkewT/LogP}$ is the CBH obtaining from Skew T/Log P diagram

$CBH_{ceilometer}$ is the CBH obtaining from ceilometer

N is the number of data

5.1.2 Coefficient of determination (R-square: R^2)

R^2 shows how well the plot of measured versus simulated data fits the 1:1 line. If the value reach to 100, it is considered acceptable performance, whereas the value reach to 0, we indicate unacceptable performance.

$$R^2 = 1 - \left[\frac{\sum_{i=1}^N (CBH_{ceilometer} - CBH_{SkewT/LogP})^2}{\sum_{i=1}^N (CBH_{ceilometer} - \overline{CBH}_{ceilometer})^2} \right] \times 100\% \quad (7)$$

where $CBH_{SkewT/LogP}$ is the CBH obtaining from Skew T/Log P diagram

$CBH_{ceilometer}$ is the CBH obtaining from ceilometer

$\overline{CBH}_{ceilometer}$ is the average CBH obtaining from ceilometer

5.2 Comparison of CBH obtained from ceilometer and MODIS

5.2.1 Mean bias deviation (MBD)

MBD shows the deviation or difference between expected and measured value. The most accurate model has an MBD value closed to zero. Generally, MBD can give negative and positive value; a negative value means that the model underestimates, while a positive value means the model overestimate.

$$MBD = \frac{\sum_{i=1}^N (CBH_{MODIS} - CBH_{ceilometer})}{\frac{\sum_{i=1}^N CBH_{ceilometer}}{N}} \times 100\% \quad (8)$$

where CBH_{MODIS} is the CBH obtaining from MODIS

$CBH_{ceilometer}$ is the CBH obtaining from ceilometer

N is the number of data

5.2.2 Coefficient of determination (R-square: R^2)

R^2 shows how well the plot of measured versus simulated data fits the 1:1 line. If the value reach to 100, it is considered acceptable performance, whereas the value reach to 0, we indicate unacceptable performance.

$$R^2 = 1 - \left[\frac{\sum_{i=1}^N (CBH_{ceilometer} - CBH_{MODIS})^2}{\sum_{i=1}^N (CBH_{ceilometer} - \overline{CBH_{ceilometer}})^2} \right] \times 100\% \quad (10)$$

where CBH_{MODIS} is the CBH obtaining from MODIS

$CBH_{ceilometer}$ is the CBH obtaining from ceilometer

$\overline{CBH_{ceilometer}}$ is the average CBH obtaining from ceilometer

CHAPTER 4

Results and discussions

4.1 Cloud vertical structure (CVS)

CBH detection by ceilometer provided information on the CVS, although we lack cloud top height (CTH) data. Ceilometer could measure up to consecutive four layers of clouds, therefore the CVS studying shows the frequency of four aggregated layers, multi-layered (two-layered and three-layered), and single-layered of clouds in different filled pattern pie chart.

During September 2016 to December 2017, as seen in Fig. 38, the most frequent detected layer was single-layered cases with 79.81%, while ceilometer detected all four aggregated layers of clouds at 0.33% and 19.86% were multi-layered (2.72% for three-layered and 17.14% for two-layered cases).

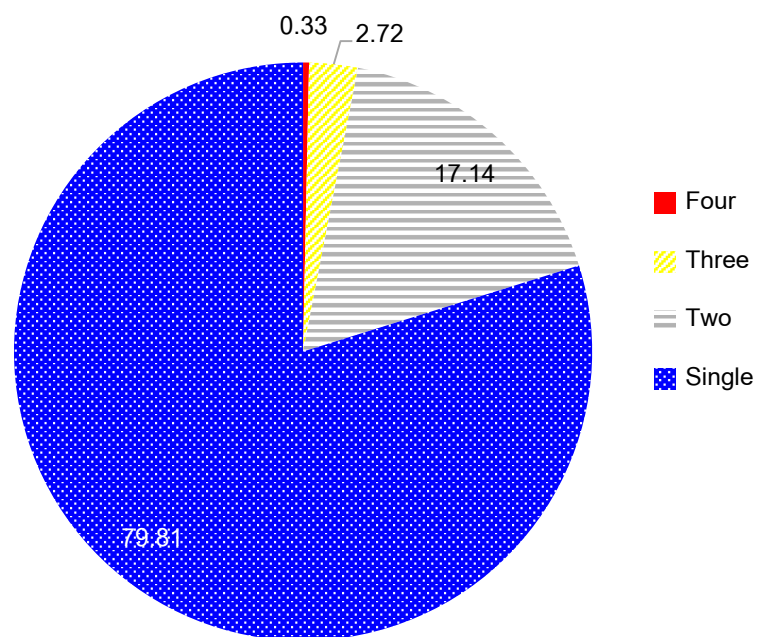


Figure 38. The frequency (%) of CBH aggregated layers, four-layered (red), three-layered (yellow), two-layered (grey), and single-layered (blue)

When we investigated CVS in different seasons, the results were illustrated in Fig. 39. In summer condition during March 2017 to April 2017, the most frequent CBH was first layer, whereas the higher layers of CBH were found frequently in winter (during November 2016 to February 2017 and November 2017 to December 2017) and rainy season (September 2016 to October 2016 and July 2017 to October 2017). There was a slight different between CBH in winter and rainy; however rainy was covered by the most complicated layer of CBH.

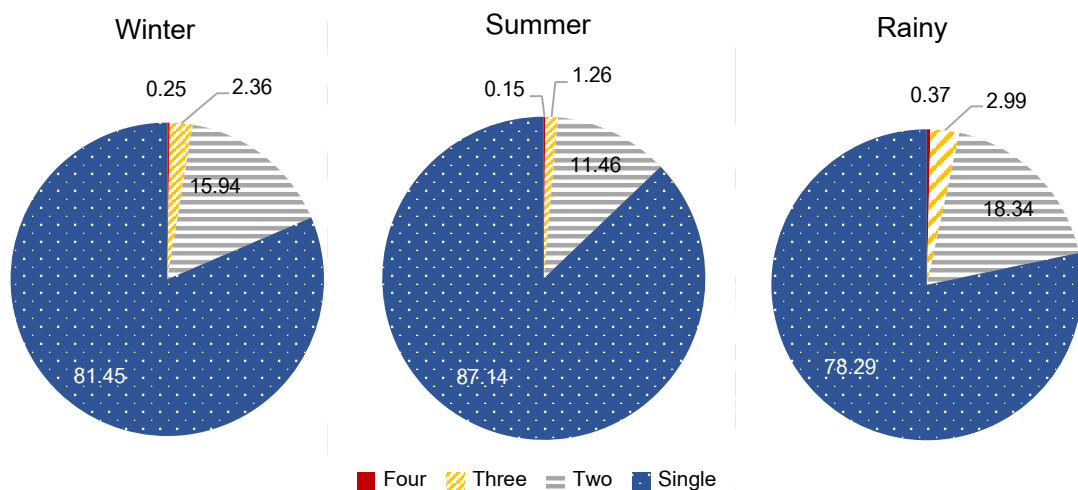


Figure 39. The frequency (%) of CBH aggregated layers, four layers (red), three-layered (yellow), two-layered (grey), and single-layered (blue) in different seasons

4.2 The CBH distributions

The CBH distributions retrieved from the ceilometer are presented in this section with the purpose of profound analysing on cloud shapes and their characteristics from September 2016 to December 2017. The illustration of the CBH frequency distribution of each layer cases covering 0 - 10 km was represented in the different filled pattern bar charts. The CBH frequency distribution for all four-layered systems was displayed in Fig. 40, the most CBH occurred under 2.5 km which was classified into low-level clouds (under 2 km) and mid-level clouds (2 - 6 km). The maximum frequency, about 45%, was approximately in the range 2 km for the first and

second layers, and the range 2.5 km was for the third and fourth layers. At upper level, it clearly noticed that there was a position of forth layers and third layers CBH. On the contrary, first layers showed more numbers as low-level type, while they gradually dropped when considered at higher altitude. As the same as second CBH characters, the most of them commonly took place at low- and mid-level of CBH, and they slowly decreased as greater distance in the atmosphere.

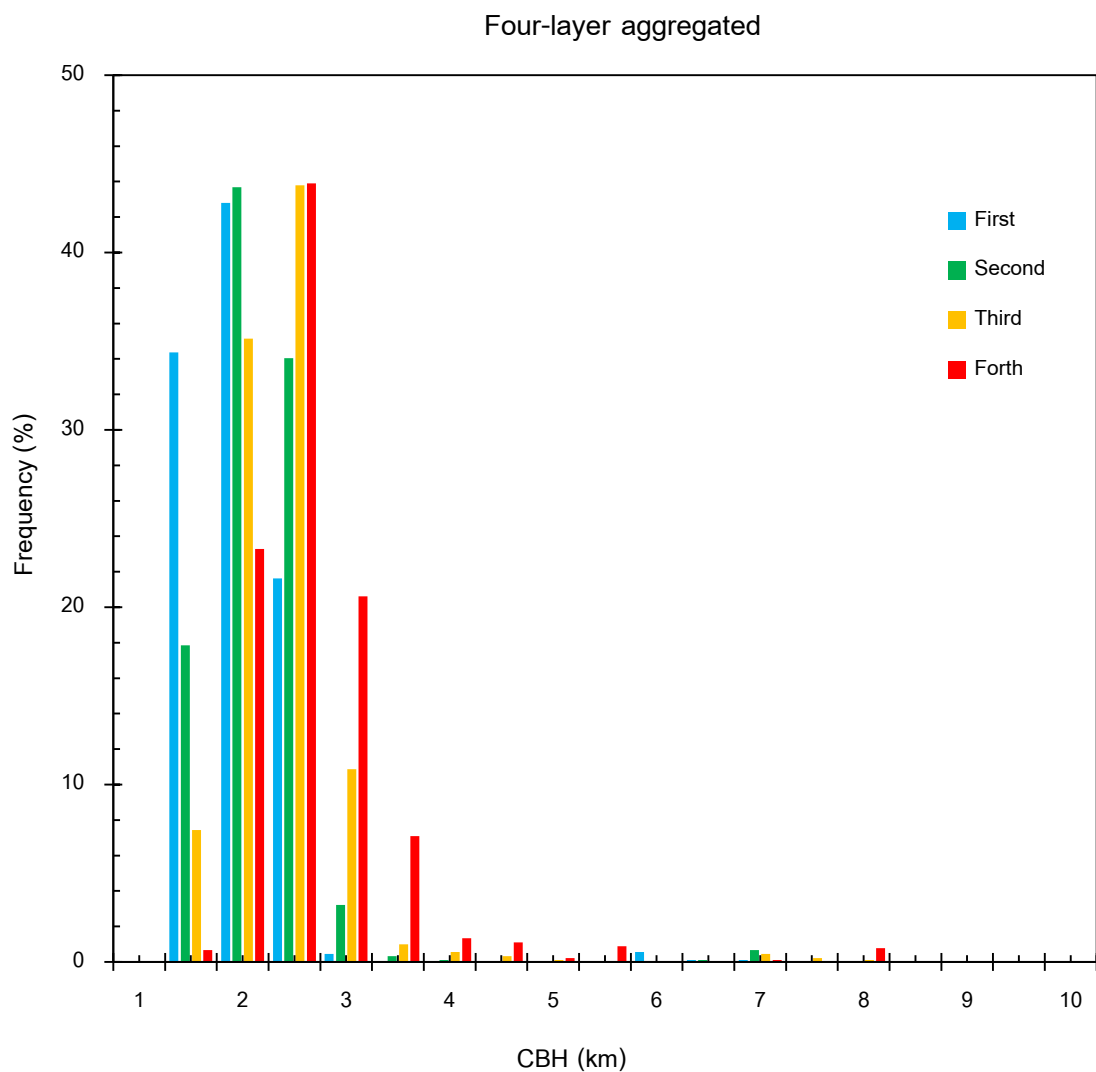


Figure 40. The CBH distribution frequency in September 2016 to December 2017 for all layers system

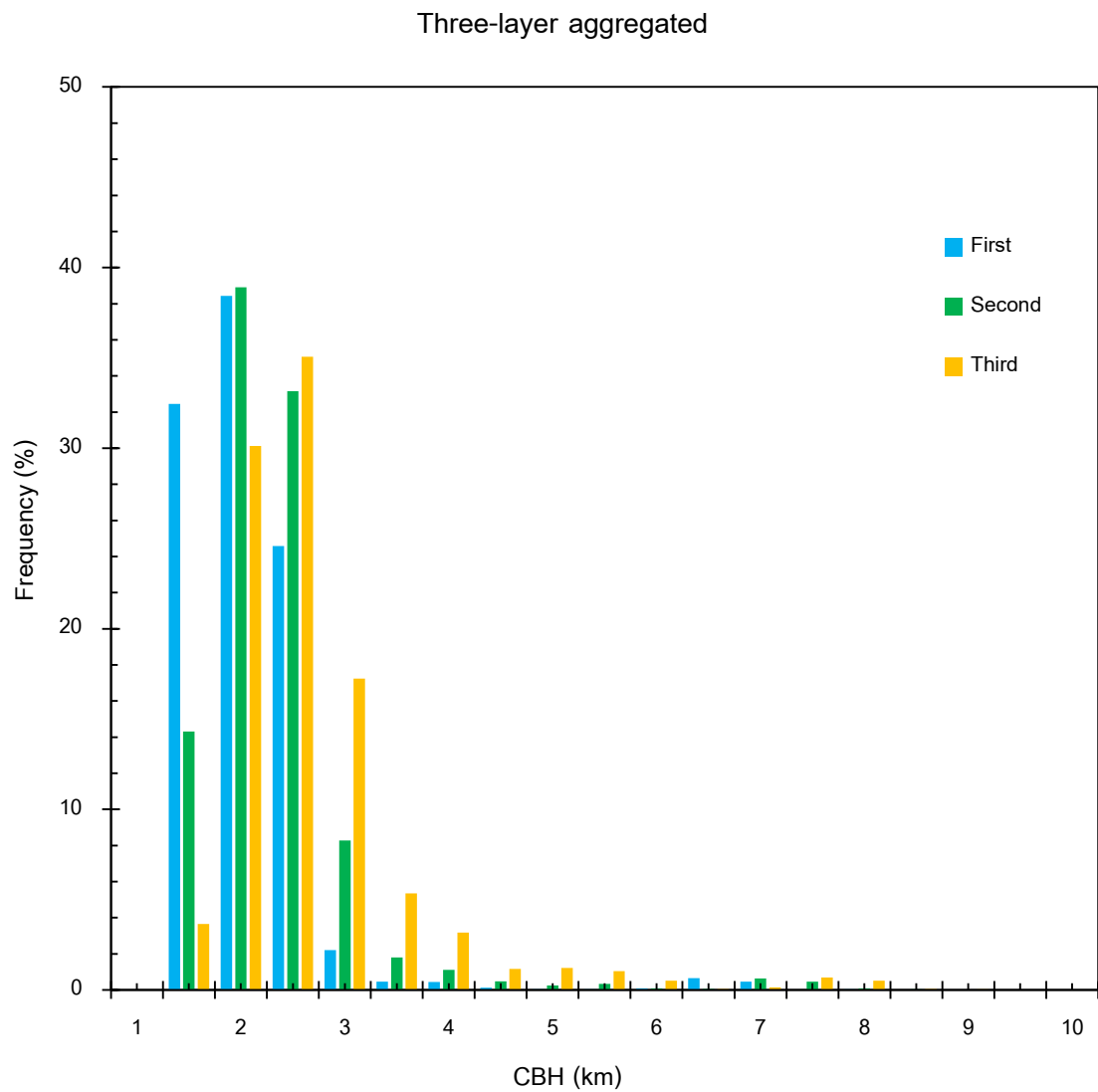


Figure 41. The CBH distribution frequency in September 2016 to December 2017 for multi-layered systems (three layers system)

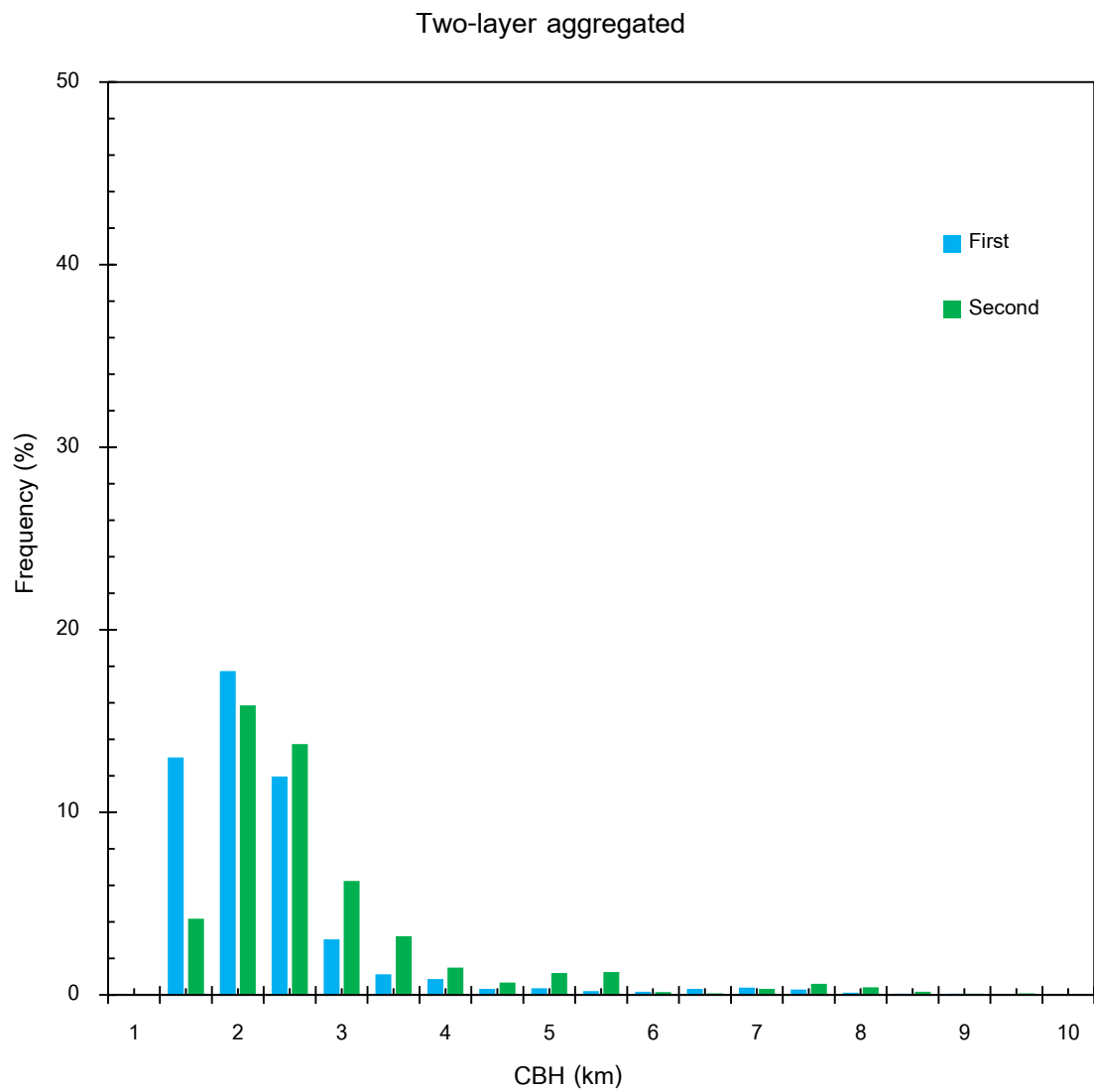


Figure 42. The CBH distribution frequency in September 2016 to December 2017 for multi-layered system (two layers system)

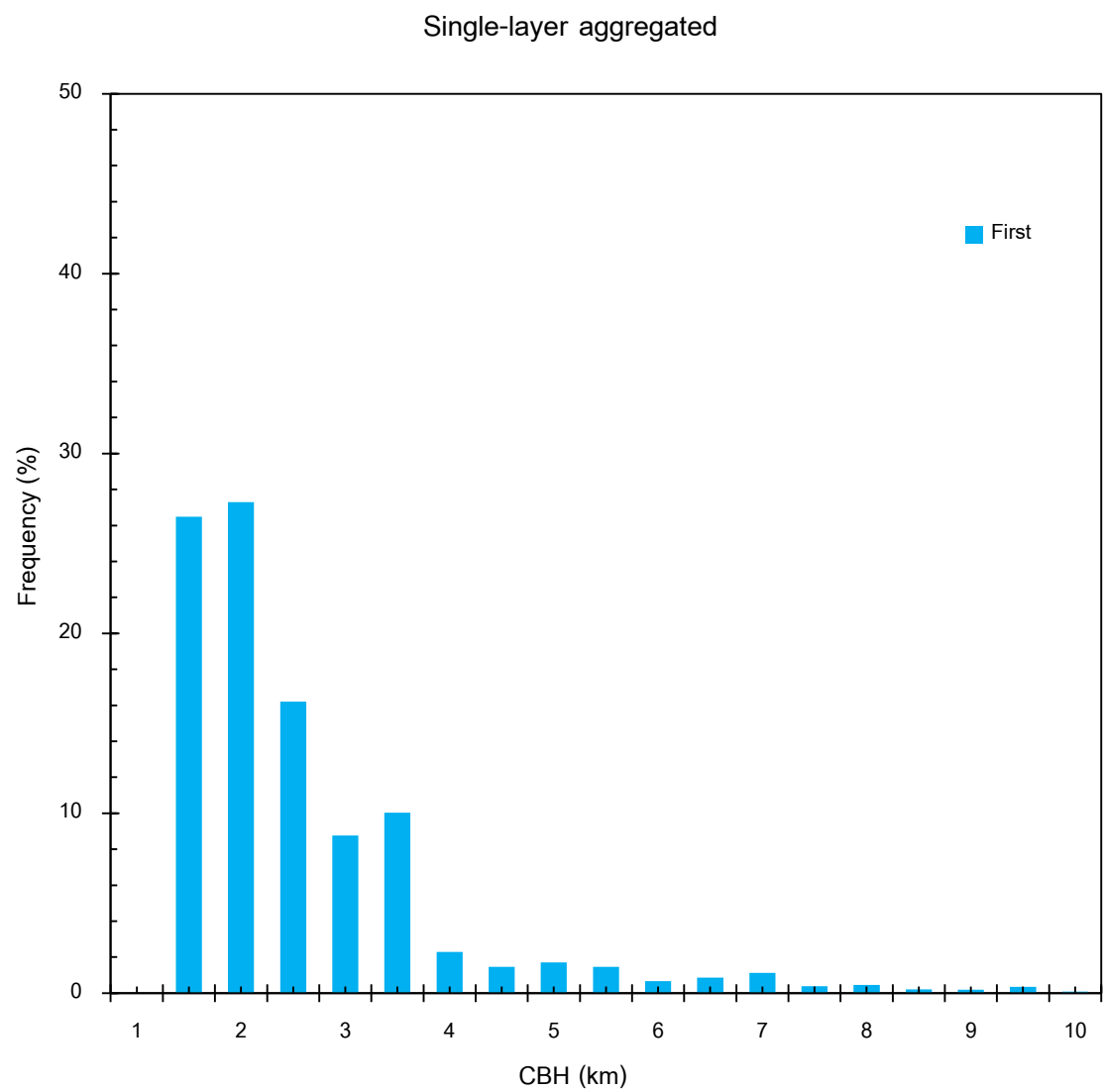


Figure 43. The CBH distribution frequency in September 2016 to December 2017 for the only first layers system

The CBH distributions in three different seasons was shown in Fig. 44., which all types of cloud (low, mid, and high) for all-layerd cases were observed over the collected site. As seen in this graph, low clouds were obviously detected as maximum in first layer of CBH, except for summer cases, while the most frequency of CBH distributions in second, third and forth CBH was accounted by middle clouds. For summer season, the middle clouds were dominant when they were detected in all of CBH layers. In contrast, the figure revealed that all types of cloud were detected during winter and rainy, but there were a slight different pattern between those seasons. The CBH layers became more complicated in rainy season, it can be seen from a flucuated level of CBH. In addition, high-level of rainy CBH occurred more often than other seasons.

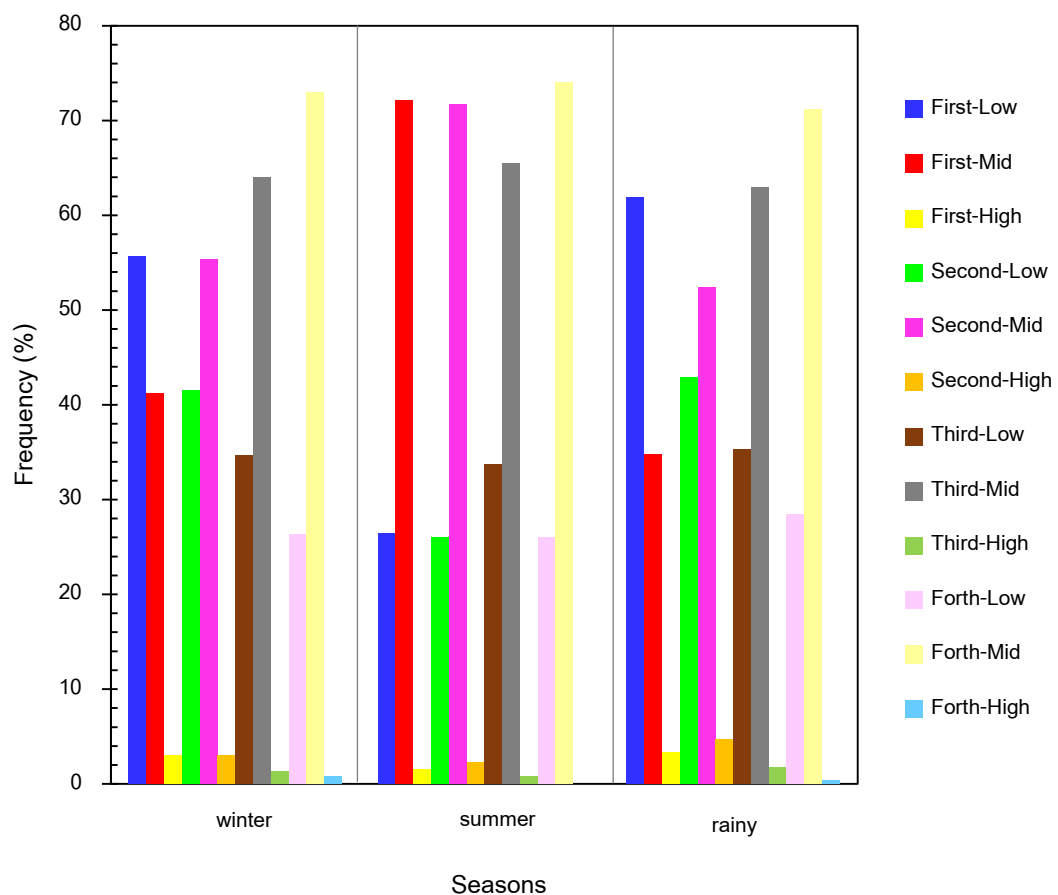


Figure 44. The CBH distributions in different seasons

Besides, the single day variation of CBH in three different seasons was shown in following figures, they were in comparable with sky image captured by sky view instrumentation, which collects every one minutes and be available during daytime only. The CBH variation for winter condition, as shown in Fig. 45, illustrated that the sky strongly covered by stratus locating near the ground level at 07:40. In the afternoon, ceilometer detection was accounted by several levels of CBH, but the higher CBH may be obstructed by the lower one.

For the convective situation in summer illustrated by Fig 46, the high-level CBH was searched in the morning and nightfall because of convection process due to heat. There was no cloud at 7:00 when the clear sky was taken by hemispheric sky view camera. Also, the low multiple CBH was captured at noon as seen in the group of broken clouds, while the higher CBH appearance happened lately in the evening until the end of the day.

Fig 47 showed the CBH variation in wet season, overall the number of multiple and forth layers of CBH increased more than other seasons. In the morning, at 07:15, there was low-level CBH when it was raining, while many types and levels of CBH were found at 10:42. In the end of the day, CBH occurrence was shown by all layer aggregated, although the sky camera was not able to detect obviously. After that, there were broken clouds spreading out through the sky in the evening.

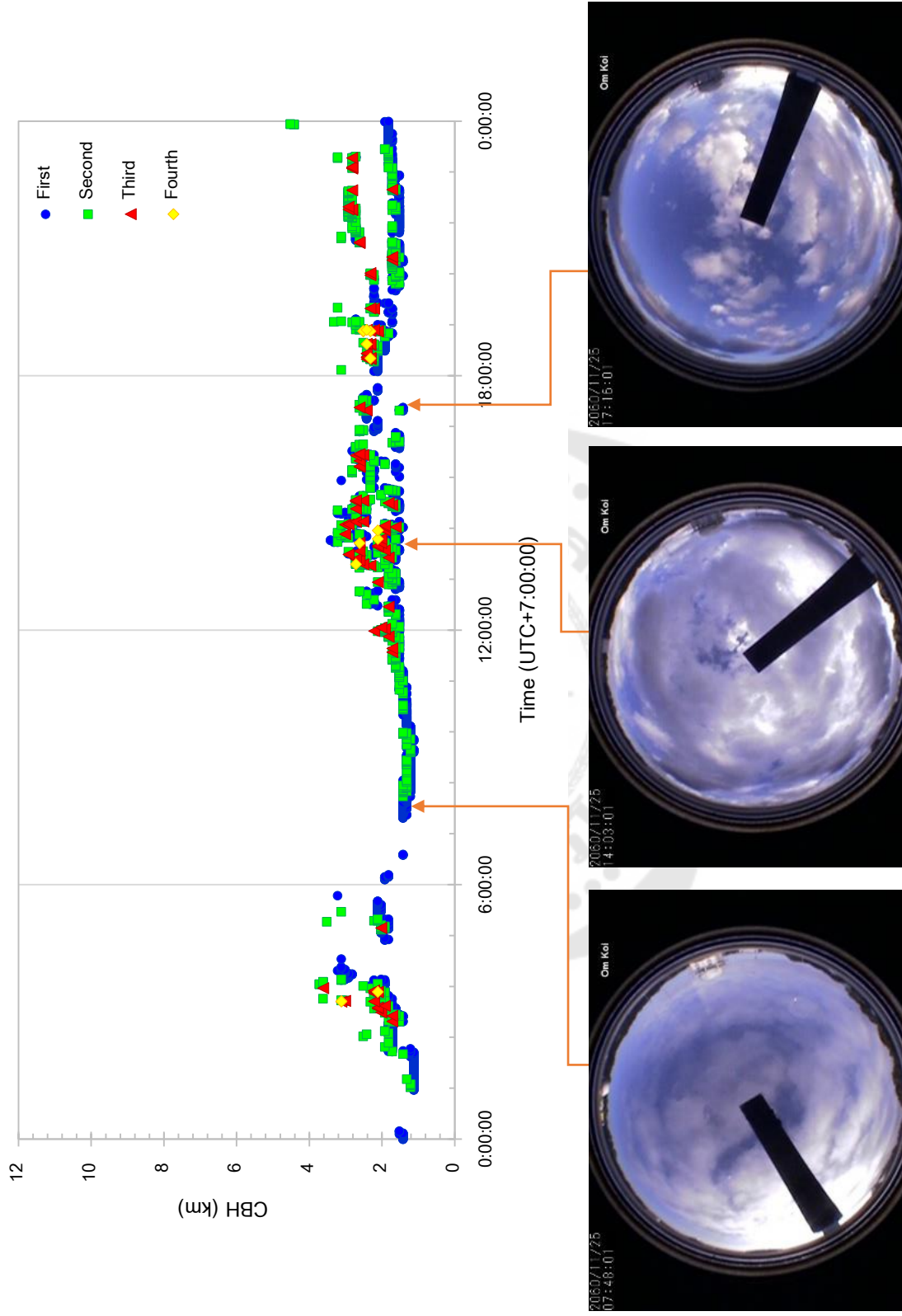


Figure 45. The single day variation of CBH in winter on November 25, 2017

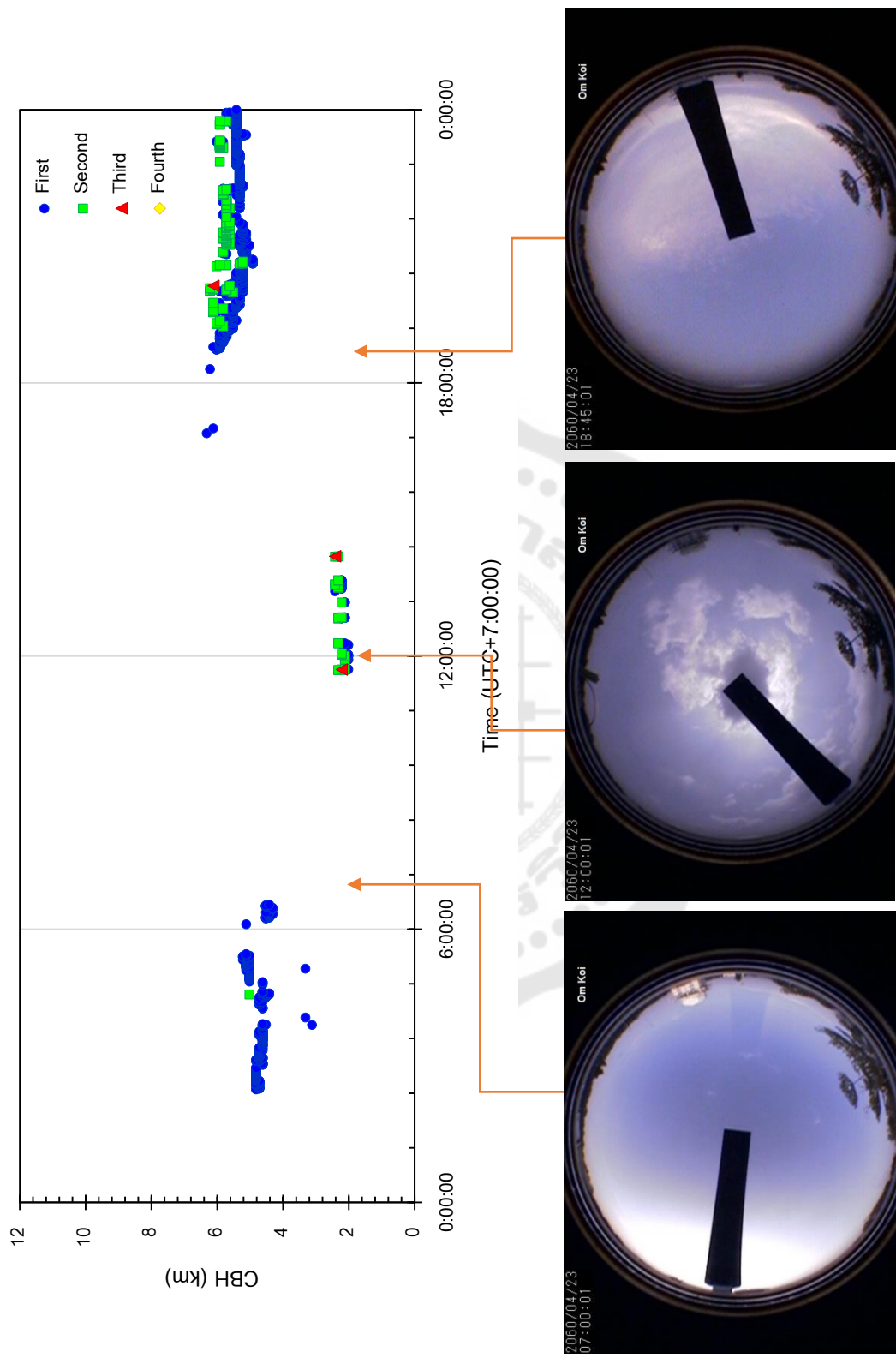


Figure 46. The single day variation of CBH in summer on April 23, 2017

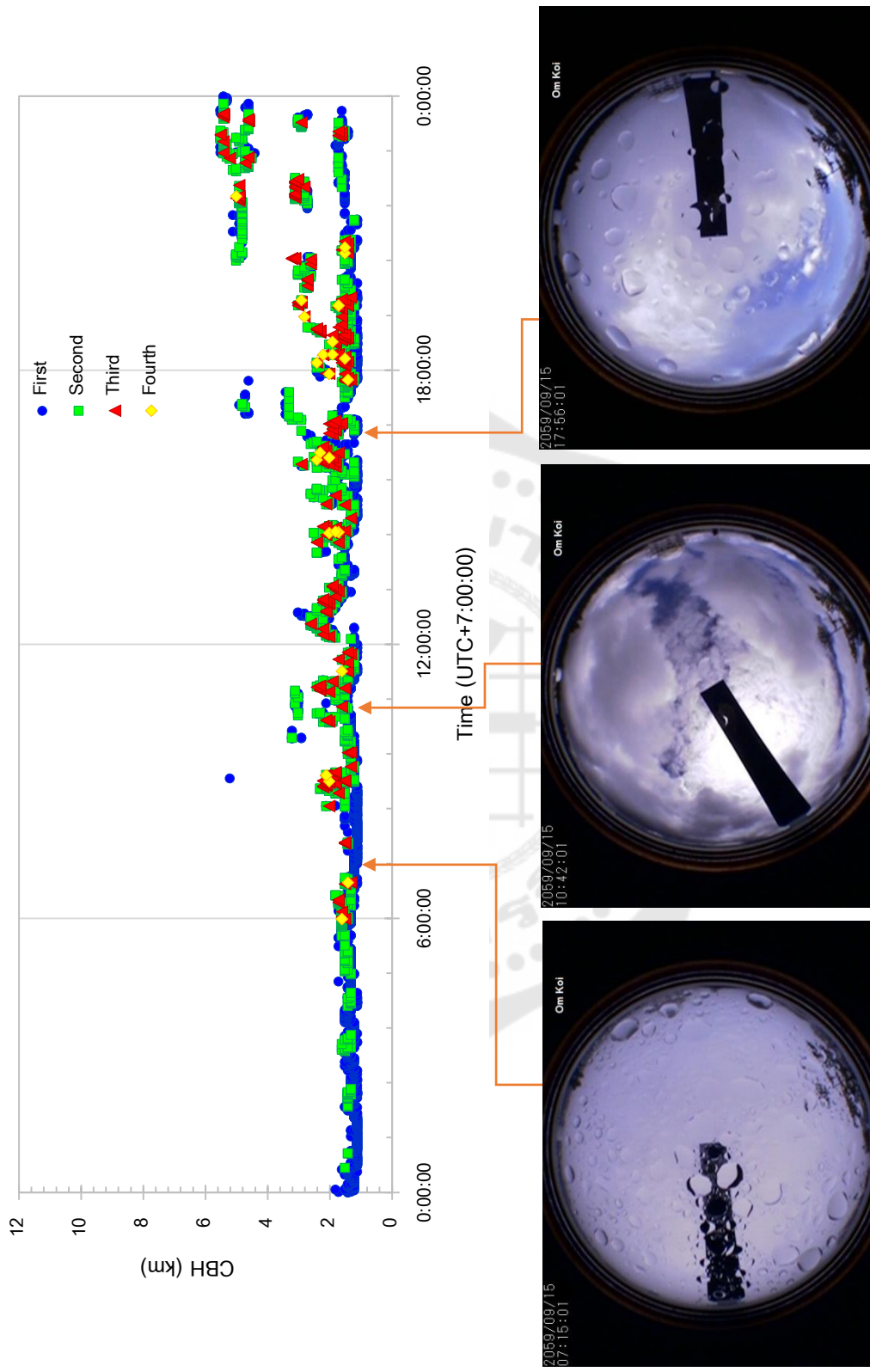


Figure 47. The single day variation of CBH in rainy on September 15, 2016

Due to the practical launching radiosonde, the inspector always ascends balloon in the morning in order to predict atmospheric conditions in next few hours. Therefore, the variation of CBH characteristics during early morning retrieved by CCL values, represented in Fig. 48, were investigated to study CBH occurrence over Chiang Mai. Morning average CBH was counted among 06:30-07:30 LCT. Overall, the most frequency of CBH occurrence was low-level cloud, which is located under 2 km; however, there was a fluctuate trend between low- to high-level clouds whole the year. During hot and cold season made large CBH variation, while during monsoon observed no major variation. Although CBH was detected at the highest altitude in cold weather, the most CBH variation was made by summer season.

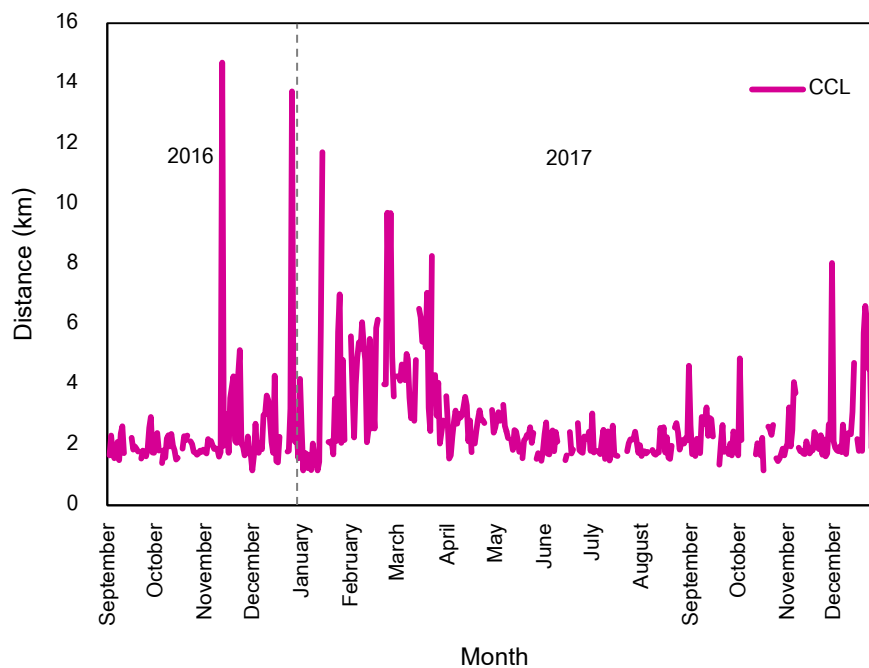


Figure 48. The variation of CBH characteristics during morning (06:30-07:30 LCT)

4.3 The distance between adjacent CBH

For multilayered cloud aggregation, distances between consecutive layers of CBH were measured to examine cloud characteristics. For CBH in 3-layered aggregated, the magenta bar represents the frequency of 3rd-2nd layers while the green striped bar represents the frequency of 2nd-1st. In contrast, the different CBH in 2-layered aggregated was shown by the blue hollow bar. As a result, the different distances varied from a range of 0.1 – 8.7 km. For three adjacent layers, the distance between 3rd-2nd layer was less than 400 m at 37.9% and 2nd-1st layer at 39.42%, as the same trend as two adjacent layers of CBH, the difference layers were below 400 m at 65.07%. In addition, the mean of distance between adjacent CBH for three-layered clouds was at 381 m and 448 m for 2nd-1st and 3rd-2nd, respectively, while 610 m was the mean for two-layered system.

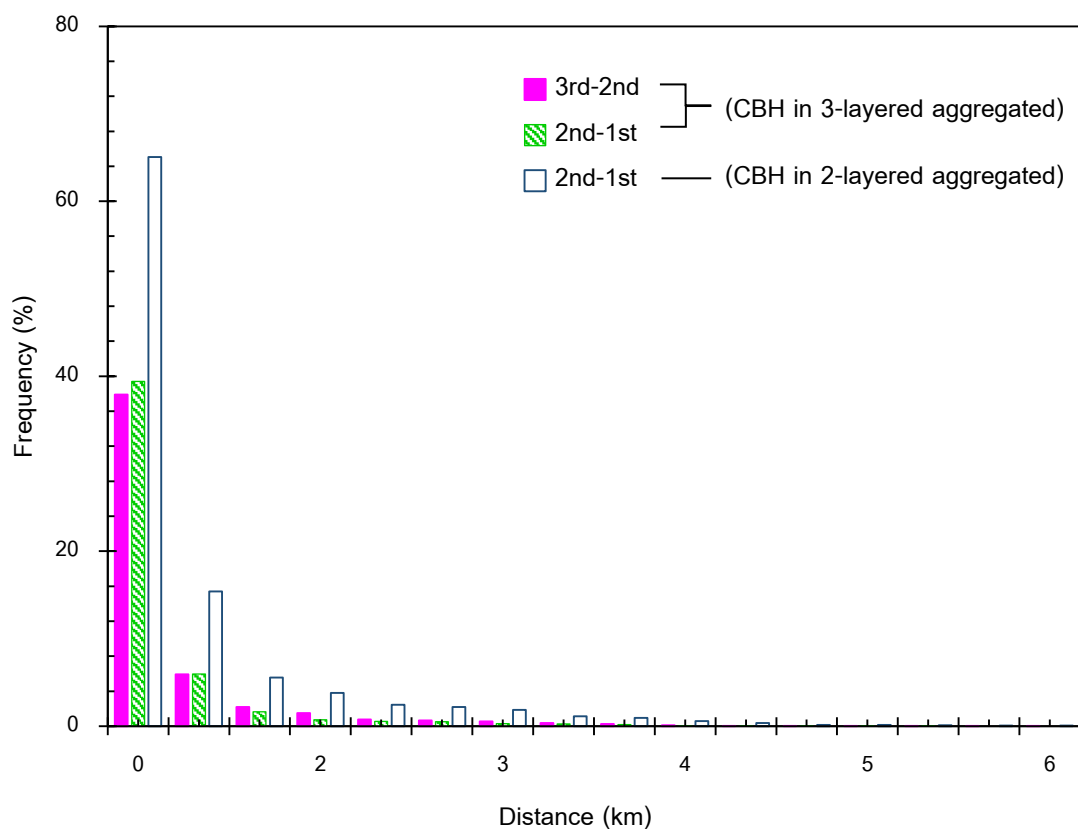


Figure 49. The frequency of distance between adjacent CBH for multilayers system

4.4 Comparison of CBH obtained from ceilometer and SkewT/LogP diagram

The ceilometer provides a real time CBH information, while the SkewT/LogP diagram is able to illustrate the theoretical CBH value and predicts the cloud base occurrence. We then compared the performance of these two methods by two statistical tests: MBD and R^2 . In this study, the observer launched radiosonde balloon into the atmosphere around 6:30-7:30 LCT (UTC+7:00) once a day, while ceilometer was a continuous instrument. Therefore, the retrieved CBH from ceilometer was in the average value compared with those from SkewT/LogP at that matching period. Yet, the lack of CBH dataset may exist due to technical problem or poor weather.

To identify where CBH is, by SkewT/LogP diagram, we need to find either CCL or LCL where the condensation could occur. We compared CBH at CCL and LCL with one derived by ceilometer in order to confirm that which value (CCL or LCL) could become more exactly CBH. According to Fig. 50 and Fig. 51, the CBH at CCL 50 mb was more credible than CBH at LCL upon the same pressure of this region. Furthermore the validation was confirmed by statistical test at MBD = 50.928, $R^2 = 0.160$ and MBD = 7.906, $R^2 = 0.281$ for LCL and CCL respectively. Besides, we noticed the CBH derived from LCL and CCL were little different which CBH at CCL was slightly higher than LCL in accordance with table 6.

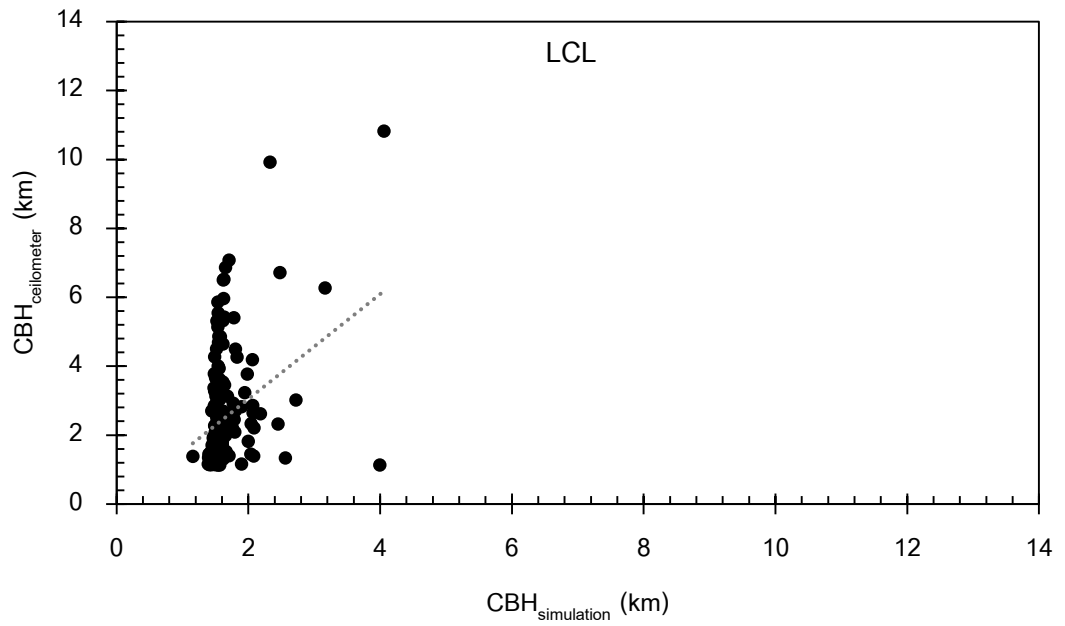


Figure 50. The linear correlation between CBH retrieved from ceilometer vs. cloud simulation at LCL 50 mb

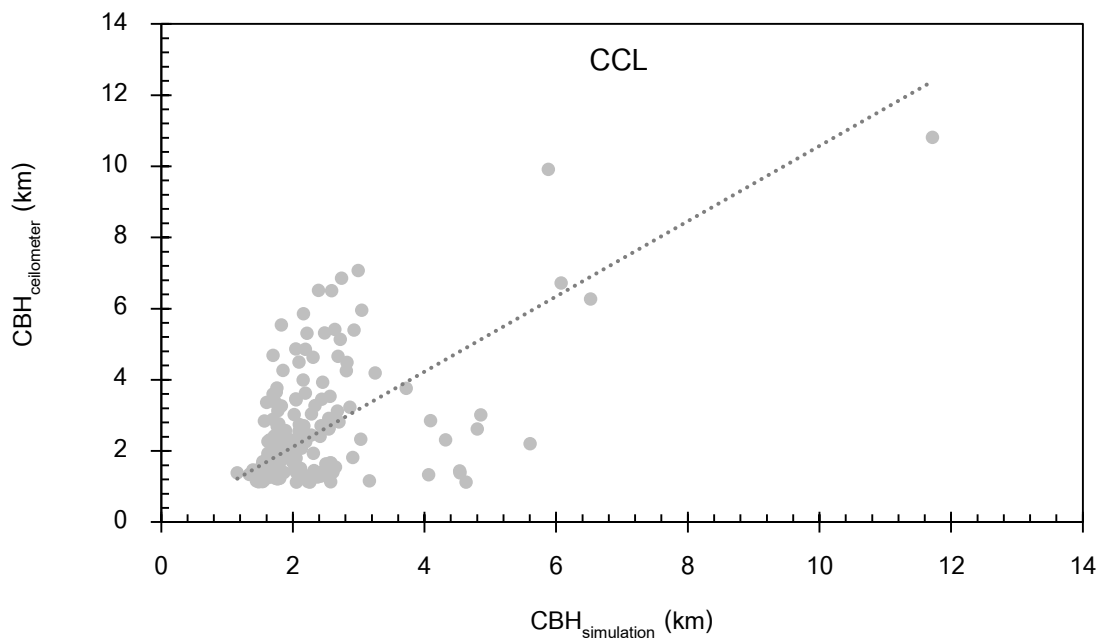


Figure 51. The linear correlation between CBH retrieved from ceilometer vs. cloud simulation at CCL 50 mb

Table 6. The example results derived from SkewT/LogP on September 2016 when LCL and CCL were in a comparison.

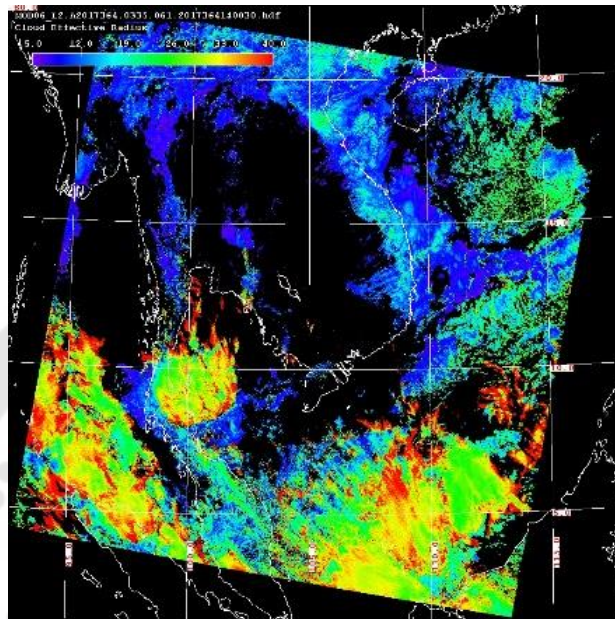
| Date | LCL (m) | CCL (m) |
|-----------|----------|----------|
| 9/2/2016 | 1520.038 | 1846.174 |
| 9/3/2016 | 1497.178 | 1814.170 |
| 9/4/2016 | 1548.079 | 1840.992 |
| 9/5/2016 | 1447.221 | 1747.114 |
| 9/6/2016 | 1477.061 | 1858.061 |
| 9/7/2016 | 1483.157 | 1830.019 |
| 9/8/2016 | 1441.125 | 1780.032 |
| 9/11/2016 | 1481.023 | 1773.022 |
| 9/17/2016 | 1474.013 | 1714.195 |
| 9/20/2016 | 1491.082 | 1789.176 |
| 9/22/2016 | 1431.950 | 1680.972 |
| 9/23/2016 | 1525.219 | 1776.070 |
| 9/24/2016 | 1494.130 | 1765.097 |
| 9/25/2016 | 1488.948 | 1716.024 |
| 9/26/2016 | 1491.996 | 1745.010 |
| 9/27/2016 | 1615.135 | 1938.223 |
| 9/30/2016 | 1543.202 | 1780.946 |

4.5 Comparison of CBH obtained from ceilometer and MODIS

MODIS is the equipment which is launched into the Earth's orbit by two satellite; Terra and Aqua. The main difference properties between Terra and Aqua is time when they pass through this area. In this work then employed two satellite working for more available data, and we compared the performance of these two methods by two

statistical tests: MBD and R^2 . Fig. 52 showed the example results retrieving from Terra and Aqua in the different time.

(a)



(b)

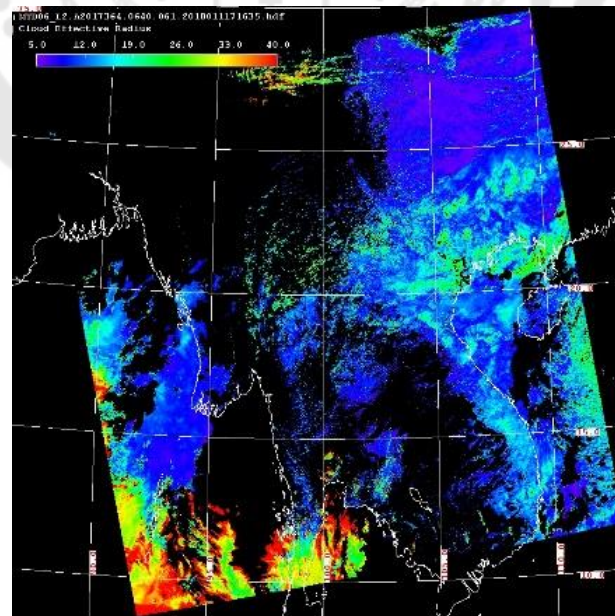


Figure 52. The received example result, cloud effective radius, by a) Terra and b) Aqua on December 30, 2017 at different time

As seen in Fig. 53, the CBH from MODIS was normally higher than the one collected by ceilometer. The whole year correlation between ceilometer and MODIS were disagreement with $MBD = -231.772$ and $R^2 = -0.281$. However, we remarked that the algorithm was valid for low- and mid-level clouds, thus we compared the CBH at that level (approximately under 3 km) from those two instruments. The results were in a good reasonable agreement with $MBD = 19.194$ and $R^2 = 0.700$, as seen in Fig. 54.

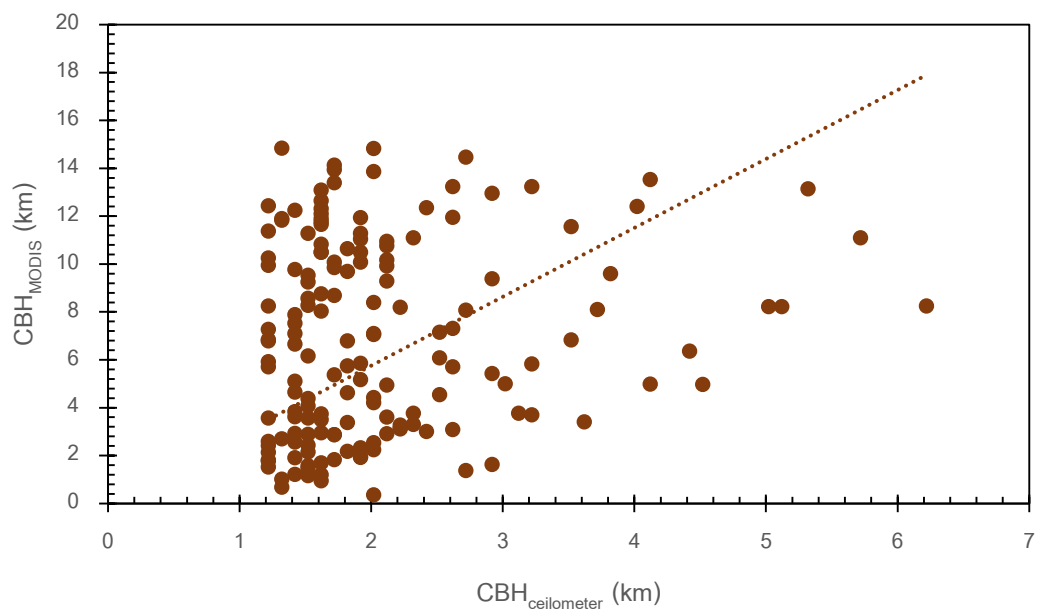


Figure 53. The linear correlation between CBH retrieved from ceilometer vs. MODIS

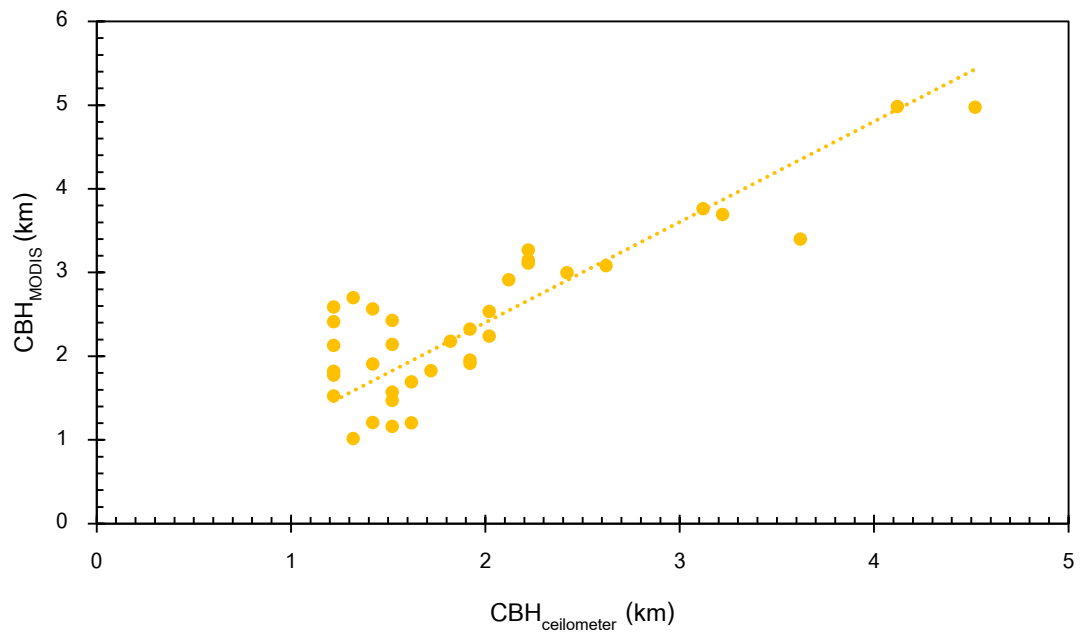


Figure 54. The linear correlation between CBH retrieved from ceilometer vs. MODIS when we considered CBH at low level

The evaluated performance of MODIS was confirmed by the following figures that CBH algorithm was valid when we consider CBH at low altitude. Fig. 55 presents CBH retrieved by ceilometer and MODIS on September 3, 2016, MODIS algorithm derived CBH at around 9.5 km, at approximately 12.00 LCT, which not related with the one detected by ceilometer. In contrast, CBH from both methods were valid when CBH algorithm derived cloud base altitude at lower level, approximately under 3 km, as seen in Fig 55.

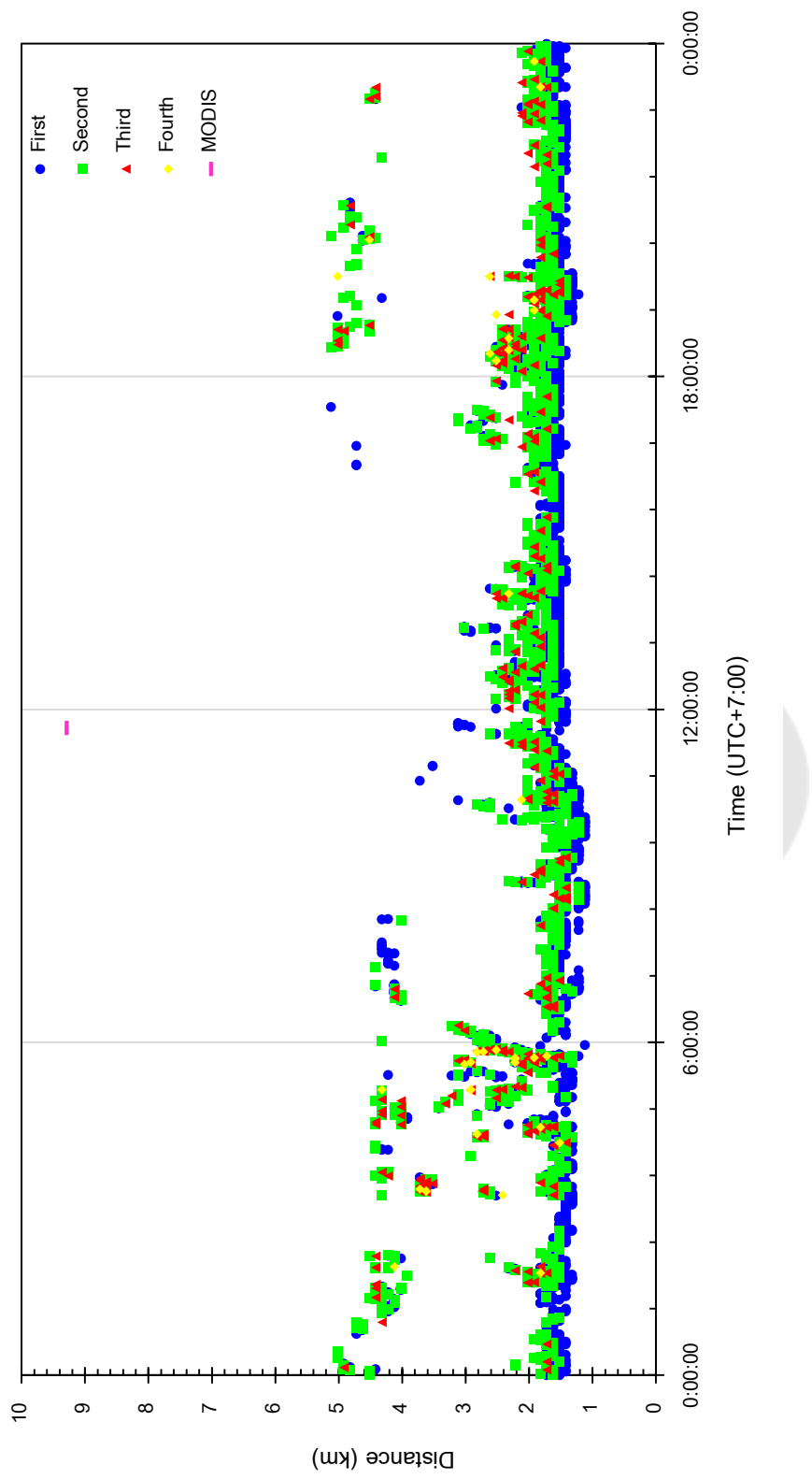


Figure 55. The comparison of CBH distribution collected by ceilometer and MODIS on September 3, 2016

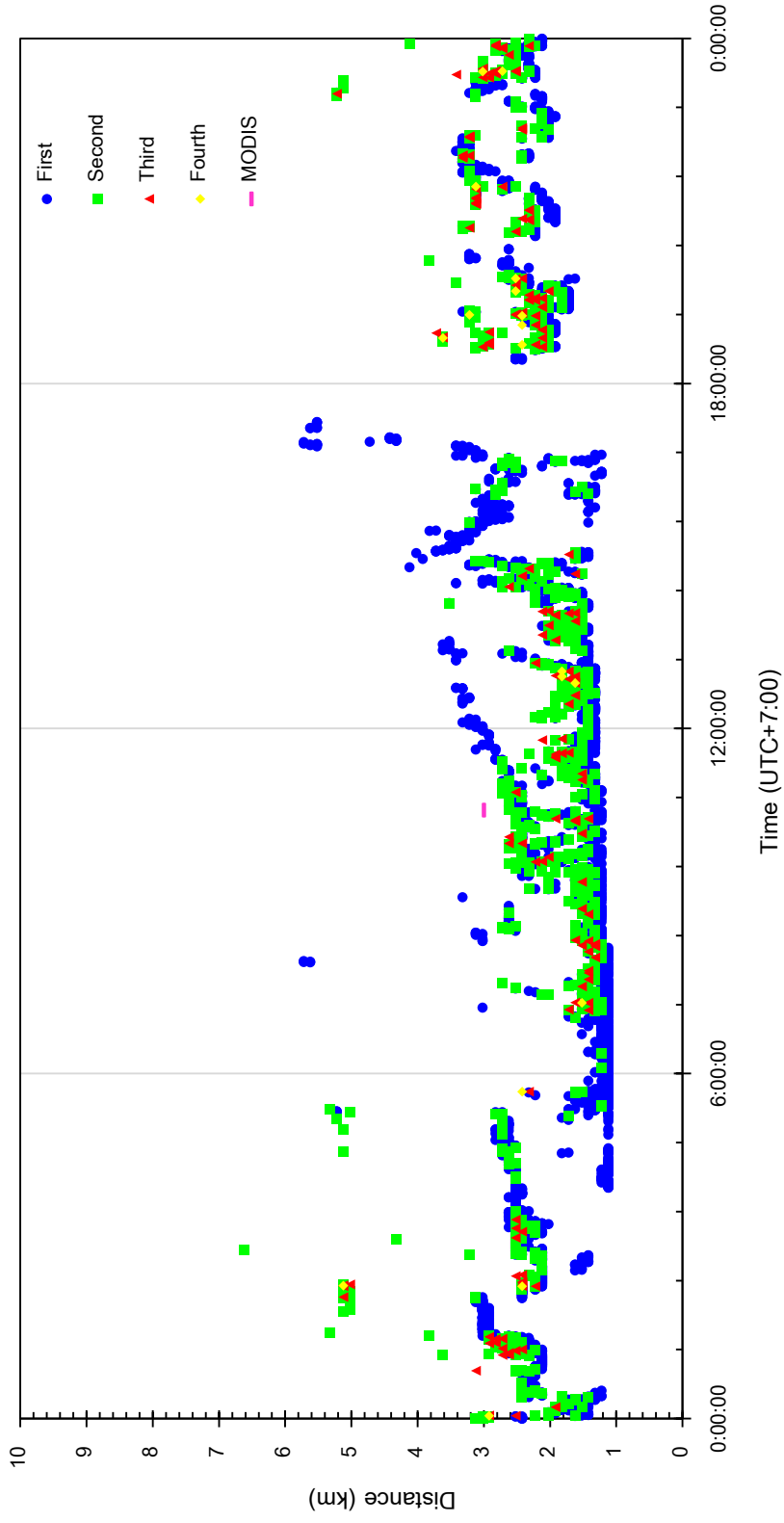


Figure 56. The comparison of CBH distribution collected by ceilometer and MODIS on September 22, 2016

CHAPTER 5

Conclusion remarks

5.1 Conclusion remarks

This thesis detected CBH from three different kinds of methods; ground-based instrument, meteorological model simulation, and satellite-based observation which were ceilometer, SkewT/LogP diagram, and MODIS satellite, respectively. Also, we compared the CBH from those three methods for validating and evaluating the performance of each approaches. Moreover, we provided the dataset of CBH over Chiang Mai for applying in Meteorology or aviation. Ceilometer can perform up to four consecutive CBH layers and provided CVS information over this site. The ceilometer observation showed that the most number of detected layers was accounted by single-layered and followed by second-layered system. The recent studies, which showed the familiar results, found that the most frequent CBH layers observed by ceilometer over Nagqu were single-layered with 65% (Song et al., 2017). As the same as Wang's work, the CVS observation during 20-year global rawinsonde dataset showed that the frequency of 1-layered, 2-layered, 3-layered, and more than three layers over land cases were 63%, 27%, 7%, and 3%, respectively (J. Wang et al., 2000). Moreover, the CBH distributions over Chiang Mai were dominated by low and middle clouds. Also, Zhang et al. investigated that the frequency over 70% of CBH were located at low levels over Tibetan Plateau, Pearl River Delta and Sichuan Basin (Zhang et al., 2018). Although ceilometer could measure up to four consecutive layers of CBH, it would rather show that signal decrease importantly due to lower cloud droplets absorption. Therefore, the lower CBH was overestimate, but the higher one was underestimate (Rémillard et al., 2012). Considering CBH in three different seasons found that Rainy season had the most complicated CBH as seen in a fluctuated level of CBH influenced by South-West monsoon that brings the land moisture above the ocean. In the other words, rainy cloud movements are influenced by gusts. For winter cases, the climate was influenced by North-East monsoon that brings cooler temperatures and generally less humidity from

China across the land site. There was a high percentage of mid- and high-clouds, it may assume that winter clouds require more moisture to form cloud base, so they rise moderately before condensing when they gain enough water vapor. Higher temperature in summer causes cloud occurring at higher altitude. It may conclude that cloud condensation process could not begin at lower distance, higher temperature, so water vapors rise gradually until they reach the condensation level as a result of greater percentage in high-level CBH. Furthermore, the CBH characteristics variation during early morning retrieved by CCL values showed that the most frequency of CBH occurrence was low-level cloud. During pre-monsoon and post-monsoon period, the higher CBH was observed more frequent than the one detected during monsoon. It gave the similar results as CBH retrieved by ceilometer over Western India (Vaishnav et al., 2019). Ceilometer is a continuous instrument providing the CVS information with real time observation while SkewT/LogP is a pseudo-adiabatic diagram with the verified assumption on the latent heat of condensation. For SkewT/LogP diagram, we could identify CBH at two level called CCL and LCL. The former is the level where CBH condenses by convective process that the air rises until the surface temperature warms and reaches this level, while the later is the level at which a parcel becomes saturated occurred by forced lifting. We found that CCL was more accurate being CBH than LCL when validated by two statistical test. It could assume that thermal convection had a stronger influence in CBH occurrence in Northern Thailand and the occurrence depend on relative humidity and temperature near the surface. Furthermore, we also noticed that LCL for a surface parcel was almost always found below the CCL, as seen in table 6, because the air must first warm before rising to the CCL (Haby, 2019). The received CBH from ceilometer and CCL simulation methods were in good correlation. However, there was slightly different which could cause by technical problem from the ascending of radiosonde, being influenced by wind profile (M. Costa-Surós et al., 2014). In addition, the inspector unfortunately did not launch the ceilometer as close as the balloon releasing location, and the characters of the planetary boundary layer, where is the lowest troposphere layer, which depend on air temperature and dew point can

change unexpectedly during the day, so the theoretical SkewT/LogP values could not perfectly model the sky and CBH, giving an unexpected error in the final results. Ceilometer is a bottom-up instrument and provides information on up to four adjacent layers of clouds which are not possible to detect by the MODIS satellite. MODIS cannot alllow CBH directly, we then need CBH algorithm which employs important parameters from MODIS such as cloud top height, cloud liquid water path, or cloud liquid water content. As a top-down instrument, the retrieved CBH from MODIS is normally detected higher than the one obtained by the standard instrument ceilometer, except for low-level CBH (approximately under 3 km). In summary, the comparison of CBH from satellite-based measurement with one of the ground-based observations suggests that the low- and mid-level clouds are much better and accurately measured by ceilometer, and the satellite reveals precisely high-level CBH due to their performances. Unfortunately, MODIS can observe in daytime only because some parameter such as liquid water path need sunlight for detecting (Sharma et al., 2016). Finally, the cloud detection could be obtained by the combination of ground-based instrument, Meteorological model simulation, and satellite-based observation which could be used for further weather modeling purposes or applications, including the potential applications on weather forecast and Meteorology. Accordingly, the correlation of obtainable and validated results from those three methods would be advantageous and practical for an enhancement of effective rainmaking, since the more accuracy CBH, the more successful cloud seeding would be accomplished.

5.2 Future works

To improve or extend this thesis, it might be done as follows;

5.2.1 Longer period and other locations may be considered for predicting continuous results in order to prepare more information.

5.2.2 Cloud formation is totally involved with RH, so we may observe the relationship between RH and cloud occurrence.

5.2.3 We could investigate CBH in other aspects such as CBH charactes on daytime and nighttime.



REFERENCES

- Ackerman, S. A., & Knox, J. A. (2007). *Meteorology: Understanding the atmosphere*.
- AIR WEATHER SERVICE SCOTT AFB IL. (1990). *The Use of the Skew T, Log P Diagram in Analysis and Forecasting. Revision*: Defense Technical Information Center.
- Battan, L. J. (1962). *Cloud physics and cloud seeding*. Garden City, N.Y.: Anchor Books.
- Bruhn, M. (2006). Stratocumulus: World Meteorological Organization.
- Bruhn, M. (2010). Fractus: WMO.
- Bureau of meteorology. (2018). Cloud Observations Study Guide. Available from Australian Government Retrieved 6 November 2018 <https://bmtc.moodle.com.au/mod/book/tool/print/index.php?id=5580#ch4109>
- Campbell scientific. (2018). CS135 Lidar Ceilometer.
- Ceilometers Net. (2015). Ceilometer Lidar for Cloud Height.
- Climate data. (n.d.). CLIMATE OMKOI. <https://en.climate-data.org/asia/thailand/chiang-mai-province/omkoi-481435/>
- Costa-Surós, M., Calbó, J., González, J. A., & Martin-Vide, J. (2013). Behavior of cloud base height from ceilometer measurements. *Atmospheric Research*, 127, 64-76. doi:<https://doi.org/10.1016/j.atmosres.2013.02.005>
- Dorr, S. T. (2018). Check out these mammatus clouds: Deborah Byrd in EARTH
- Duarte, R. P. M., & Gomes, A. J. P. (2017). Real-time simulation of cumulus clouds through SkewT/LogP diagrams. *Computers & Graphics*, 67, 103-114. doi:<https://doi.org/10.1016/j.cag.2017.06.005>
- Everson, B. (2017). cirrocumulus.
- Favre, M. (2016). Cumulonimbus alpin.
- Forsythe, J. M., Haar, T. H. V., & Reinke, D. L. (2000). Cloud-Base Height Estimates Using a Combination of Meteorological Satellite Imagery and Surface Reports. *American Meteorological Society*, 39, 2336-2347.
- Funk, T. (n.d.). Cloud Classifications and Characteristics Retrieved from <https://www.weather.gov/> website:

- Gudd, M. (2016). Altostratus radiatus (As ra): World Meteorological Organization.
- Guichard, F., & Couvreux, F. (2017). A short review of numerical cloud-resolving models. *Tellus A: Dynamic Meteorology and Oceanography*, 69(1), 1373578. doi:10.1080/16000870.2017.1373578
- Julian Mayers, & Hughes, k. (2004). *Understanding Weather : A visual approach*. Great Britain: Arnold.
- K. Holejko, & Nowak, R. (2000). Continuous wave laser ceilometer with code modulation for measurementd of cloud base height. *Opto-electronics review*, 8(2), 195-199.
- Knapp, R. (2014). Stratus. NOAA Photo Library: NOAA.
- L'Ecuyer, T., & Jiang, J. H. (2010). Touring the Atmosphere Aboard the A-Train. *Physics Today*, 63.
- Lee, S., Hwang, S.-O., Kim, J., & Ahn, M.-H. (2018). Characteristics of cloud occurrence using ceilometer measurements and its relationship to precipitation over Seoul. *Atmospheric Research*, 201, 46-57. doi:https://doi.org/10.1016/j.atmosres.2017.10.010
- Linacre, E., & Geerts, B. (n.d.). Cloud liquid water content, drop sizes, and number of droplets. from University of Wyoming http://www-das.uwyo.edu/~geerts/cwx/notes/chap08/moist_cloud.html
- Linehan, S. (2010). cumulus. NOAA Photo library: NOAA.
- Liu, L., Sun, X.-j., Liu, X.-c., Gao, T.-c., & Zhao, S.-j. (2015). Comparison of Cloud Base Height Derived from a Ground-Based Infrared Cloud Measurement and Two Ceilometers. *Advances in Meteorology*, 2015, 8. doi:10.1155/2015/853861
- Mcmurdie, L. (2007). SKEW-T, LOG-P DIAGRAM ANALYSIS PROCEDURES. Retrieved 8 July 2018, from University of washington <https://atmos.washington.edu/~mcmurdie/classes/370/skew-t/Skew-T.pdf>
- Mecelis, Á. (2015). Halo Solar.
- Met office. (2018, 21 February 2018). Weather front. Retrieved from <https://www.metoffice.gov.uk/learning/atmosphere/weather-fronts>
- Moran, & Mogan. (1997). *meteorology: the atmosphere and science of weather*.

- NASA. (2017). Terra Spacecraft.
- NASA. (2018). About Aqua.
- NASA. (n.d.). MODIS. Retrieved from <https://modis.gsfc.nasa.gov/about/>
- Nave, R. (n.d.). Blue Sky. Retrieved from <http://hyperphysics.phy-astr.gsu.edu/hbase/atmos/blusky.html>
- Newman, L. E. (2006). Moisture, Stability, and Precipitation.
- NordNordWest. (2009). Thailand Chiang Mai locator map. In T. C. M. I. map.svg (Ed.), *Thailand location map.svg* (Vol. 1,052 × 1,849 pixels, pp. Locator map of Chiang Mai Province, Thailand). Wikipedia: Wikipedia.
- Omdal, C. (2016). altocumulus. NOAA Photo Library: NOAA.
- Orange Smile. (n.d.). Detailed hi-res maps of Chiang Mai Region for download or print (Vol. 241 X 1755 pixels). <http://www.orangesmile.com>.
- Peengam, S. (2017). *A study of cloud base height and cloud cover at a tropical site in Northern Thailand*. (Master of science), Sipakorn University.
- Penry, J. (2013). Wall cloud. NOAA Photo Library: NASA.
- Pukdeekiat, P. (2016). *Determination of direct solar radiation using atmospheric physics models*. (Master of Education), Srinakharinwirot University
- Rui P.M. Duarte, & Abel J.P. Gomes. (2017). Real-time simulation of cumulus clouds through SkewT/LogP diagrams. *science direct*, 67(Computers & Graphics), 103-114.
- Russell, R. (2018). Mesosphere diagram: UCAR Center of science education.
- Schumacher, J. (2007). Cirrus.
- Schwemmer, R. (2013). fog. NOAA photo library: NASA.
- Sharma, S., Vaishnav, R., Shukla, M. V., Kumar, P., Thapliyal, P. K., Lal, S., & Acharya, Y. B. (2016). Evaluation of cloud base height measurements from Ceilometer CL31 and MODIS satellite over Ahmedabad, India. *Atmos. Meas. Tech.*, 9(2), 711–719. doi:10.5194/amt-9-711-2016
- Stefan, S., Ungureanu, I., & Grigoras, C. (2014). A survey of cloud cover over Magurele,

- Romania, Using ceilometer and satellite data. *Romanian Reports in Physics*, 66(3), 11.
- Sugi, M. (2013). nimbostratus.
- Theberge, C. A. E. (2018). contrail. NOAA Photo Library: NASA.
- Thompson, J., County, W., & Illinois. (2013). Shelf cloud over NW Illinois. NOAA Photo Library: NASA.
- Tzoumanikas, P., Nikitidou, E., Bais, A. F., & Kazantzidis, A. (2016). The effect of clouds on surface solar irradiance, based on data from an all-sky imaging system. *Renewable Energy*, 95, 314-322. doi:<https://doi.org/10.1016/j.renene.2016.04.026>
- Vaisala. (2016). *Accuracy Matters in Radiosonde Measurements*. Retrieved from
- Vongpadai, K. (2016). *THE ESTIMATIONS OF GLOBAL AND DIFFUSE SOLAR RADIATION USING ACTUAL METEOROLOGICAL DATA IN BANGKOK* (Master degree), Srinakharinwirot University.
- Wang, Y., Shi, C., Wang, C., & Xiao, B. (2018). Ground-based cloud classification by learning stable local binary patterns. *Atmospheric Research*, 207, 74-89. doi:<https://doi.org/10.1016/j.atmosres.2018.02.023>
- Wiegner, M., Madonna, F., Biniotoglou, I., Forkel, R., Gasteiger, J., Geiß, A., . . . Thomas, W. (2014). What is the benefit of ceilometers for aerosol remote sensing? An answer from EARLINET. *Atmos. Meas. Tech.*, 7(7), 1979-1997. doi:10.5194/amt-7-1979-2014
- Wither, J., Bouthors, A., & Cani, M.-P. (2008). *Rapid sketch modeling of clouds*. Paper presented at the Proceedings of the Fifth Eurographics conference on Sketch-Based Interfaces and Modeling, Annecy, France.

VITA

NAME Piyaon Sapphaphab

DATE OF BIRTH 9 September 1993

PLACE OF BIRTH Bangkok

INSTITUTIONS ATTENDED 2011 High school Satriwatrakhang School, Bangkok
2017 Bachelor Degree Srinakharinwirot University, Bangkok
2019 Master Degree Srinakharinwirot University, Bangkok

HOME ADDRESS 999/52 Banggruay-Jongthanom Rd, Bang Khanun,
Banggruay, Nonthaburi, 11130.

